# OPERA-4: On the coexistence of weather radars and wind turbines

Hidde Leijnse (KNMI), Reinhard Teschl (TU Graz),
Helmut Paulitsch (TU Graz), Franz Teschl (TU Graz),
Gemma Holmes (UKMO), and Laila Fodnes Sidselrud (met.no)

February 25, 2022

# Chapter 1

# Introduction

The transition from fossil fuel-based energy production to sustainable energy generation has spurred the development of wind turbines. Wind turbines interact with radar signals, and can therefore affect weather radar measurements (e.g. Norin, 2015; Angulo et al., 2015). With the recent and projected development of (parks of) wind turbines, it is important to re-evaluate practices regarding placement of wind turbines near weather radars (OPERA, 2006, 2010).

Wind turbines that are in the main beam of the radar (which generally occurs when these turbines are very close to the radar) can block part of the radar beam, causing a decrease in the returned power (see Fig. 1.1). Wind turbines also reflect power back to the radar. Because wind turbines are generally constructed of materials that reflect radio waves very efficiently, these reflections can be very intense and visible far from the radar.

Wind turbines or wind farms can hence have a negative influence on the quality and usefulness of weather radar data and products. Because wind turbine blades move when the wind turbine is turned on, standard ground clutter filtering will not be effective in removing these echoes. This is because standard ground clutter filtering assumes ground clutter to be stationary. Because the decrease in quality of weather radar data affects many end users in their task regarding the safety of the general public, it is necessary to coordinate the placement of wind turbines with the locations of weather radars. The impact of wind turbines in radar data on the end users' tasks is quantified in this report.

Effects of wind turbines on both the radar reflectivity factor $Z$ and mean Doppler velocity $V$ are discussed in this report. The effect on polarimetric variables such as $\rho_{HV}$, $Z_{DR}$, and $k_{DP}$ is discussed more briefly and is further considered relating to the use of these variables for the detection of wind turbines.

This report is an update of earlier OPERA reports on the effect of wind turbines on weather radar data (OPERA, 2006, 2010). It describes how wind turbines affect weather radar measurements and the impact that this has on end users (e.g. hydrologists, weather forecasters, etc.). The effectivity of efforts to mitigate the effects of wind turbines are also discussed in terms of how they affect the end users.

There are large differences in how weather radar operators in Europe are consulted with respect to the placement of wind turbines in different European countries. Such differences also exist for national guidelines used for placement

Figure 1.1: Examples of different wind turbine orientations (both hub and blades) with respect to the radar beam. Background coloring indicates the power of the beam, where white indicates the most power, and red the least. Beam powers have been computed assuming a wind turbine that is 50 m higher than the radar antenna feed, a beam elevation of 0.5°, a 1° beam width, and a distance to the radar of 2 km (left panel), 5 km (center panel), and 15 km (right panel).

of wind turbines in the vicinity of weather radars, despite existing European (OPERA, 2010) and global (WMO, 2010, Annex VI, p. 58–59) guidelines. If these guidelines are used in planning where wind turbines are places, this can be useful in reducing the impact on weather radar data quality. However, providing new European guidelines is outside the scope of this report.

# Chapter 2

# Impact of wind turbines on weather radar data

Because the size of the different parts of wind turbines is much larger than radar wavelengths ($\lambda$) typically used for weather radar ($\lambda \approx 10$ cm for S-band, $\lambda \approx 5$ cm for C-band, and $\lambda \approx 3$ cm for X-band), the scattering regime that is relevant here is the optical regime. This means that the amount of beam blockage is proportional to the physical cross-section of the turbine. For perfectly conduction cylinders (with which the different parts of the wind turbine can be approximated) the radar reflectivity factor $Z$ scales with $\lambda^3$ (e.g. Angulo et al., 2015), so that for a given wind turbine $Z$ would be 8 times as large (i.e, 9 dB larger) for an S-band radar than for a C-band radar. Note that most operational weather radars in Europe are C-band radars, but S-band and X-band radars are also used.

## 2.1 Impact on reflectivity measurements

The radar reflectivity factor ($Z$) is the radar variable that is commonly used for monitoring and short-term forecasting of severe storms (e.g. Maynard, 1945), rainfall estimation for hydrological applications (e.g. Krajewski and Smith, 2002), climate monitoring (e.g. Overeem et al., 2009), and hail monitoring with single-polarization radars (e.g. Holleman et al., 2000). It is also used for assimilation into numerical weather prediction (NWP) models (e.g. Sun et al., 2014), which are in turn used to forecast severe weather. The radar imagery presented on most websites is either $Z$ itself or a variable derived from $Z$. Any impact that wind turbines have on this variable will hence directly influence all of these application areas.

### 2.1.1 Reflection by wind turbines

Because wind turbines contain metals in both the tower and the blades (e.g. for lightning protection), they reflect radio waves very efficiently. Even when far away from a radar, wind turbines can hence cause very large radar returns (e.g OPERA, 2006, 2010; Vogt et al., 2007; Norin and Haase, 2012; Norin, 2015; Keränen et al., 2014). The severity of the radar returns caused by wind turbines

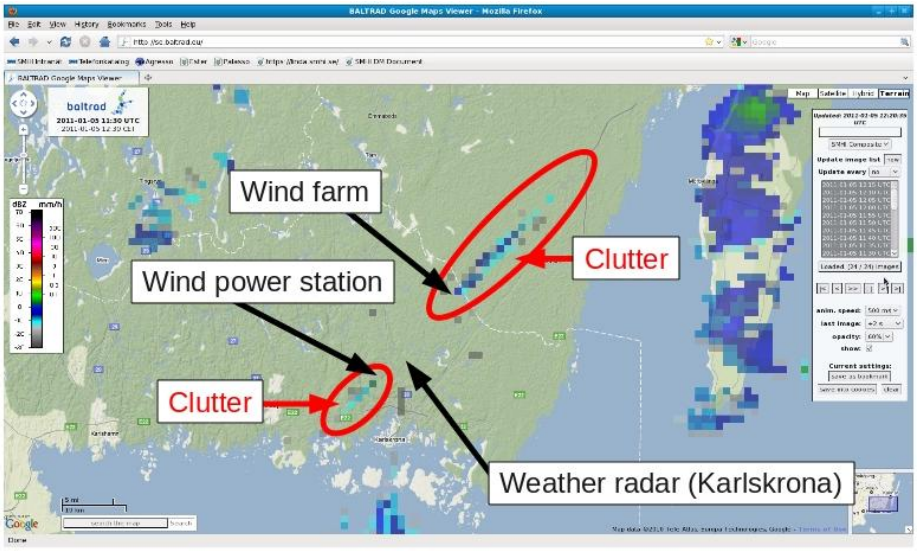


Figure 2.1: Snapshot of the BALTRAD Google Maps Viewer showing wind turbine clutter in the Swedish national reflectivity composite product. The distance between radar Karlskrona and the wind farm to the north-east (5 turbines: hub height and rotor diameter are both 100 m) is approximately 13 km while the distance to the single wind turbine to the south-west is much closer. Note the tail of reflectivities behind the wind turbines.

is expected to decrease with distance from the radar ($r$). The radar reflectivity factor $Z$ that is generally used in radar meteorology is determined from the power received by the radar by assuming that the radar measurement volume is uniformly filled with distributed targets. The fact that a wind turbine is not a distributed target means that its radar reflectivity factor decreases with $r^2$ if its radar cross-secion is invariant with range. Furthermore, generally (in relatively flat terrain) the radar beam is higher above the ground at longer ranges, so that the probability of a wind turbine being in the main beam of the radar decreases with $r$ (see Fig. 1.1). It should be noted here that antenna sidelobes may still cause significant wind turbine clutter even though the wind turbines are not in the main beam of the antenna. And anomalous propagation can cause much more wind turbine clutter than under normal propagation conditions (Hood et al., 2010).

Especially close to a radar, the area behind wind turbines may also be affected by them. This is because the radar pulse scattered by the wind turbine may hit the ground and then return to the radar via the wind turbine (three-body scattering). Such "clutter tails" may be several km long (e.g. Norin, 2015, and Fig. 2.1). The effectivity of the scattering off the ground depends on the roughness of the terrain and the local topography within several km from the wind turbine, and hence so does the severity of these clutter tails.

Radar sidelobes not only cause wind turbine reflections in scans with the main beam above the turbine location, but also cause turbine clutter in azimuth gates to the left and right of the wind turbine location. Thorough analyses of the spatial extent of clutter by wind turbines are presented in Appendix A. It

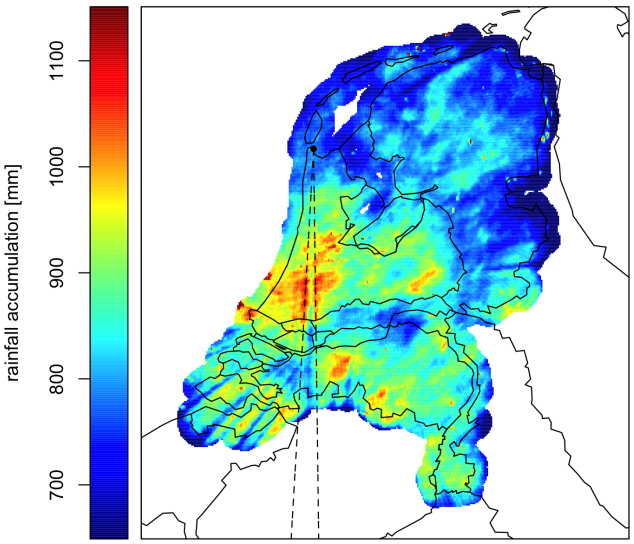


Figure 2.2: Rainfall accumulations over the Netherlands for 2016 derived from composites of two radars, and adjusted by rain gauges (Overeem et al., 2008). Two 48-m high wind turbines (Helsdeur wind farm) located at 665 m and 781 m to the south of the Den Helder C-band radar (antenna is 51 m above mean sea level) block the radar beam. The area that is blocked by the wind turbines is indicated by the dashed lines.

should be noted here that the wind turbines studied there do not show any clutter tails, possibly because they are in very flat and smooth terrain.

Several radars use the spatial texture of reflectivity or other variables (see Section 2.3) for radar echo classification (e.g. Hall et al., 2017). Texture is computed from spatial gradients, which means that also pixels adjacent to those affected by wind turbines are affected, leading to a larger area becoming less useful for meteorological applications.

The strength of clutter signals from wind turbines depends greatly on the location and orientation with respect to the radar (see e.g. Fig. 1.1), and the speed of the blades. It is shown in Appendix A that for a wind farm 16 km from a radar, the *average* reflectivity over a 2-year period may be close to 40 dBZ. It is clear from Figs 12 and 28 of this appendix that high reflectivity factors (even up to 65 dBZ) occur more than 10 times more often in pixels affected by wind turbines than in pixels not affected by wind turbines. This effectively means that wind turbines can yield extremely high radar returns, and that these radar returns occur much more often than weather that generates similar reflectivities.

### 2.1.2 Beam blocking by wind turbines

A wind turbine that extends into the main beam of the radar will block a part of the radiation, and hence cast a "shadow" behind it. The effect of this is that less power is returned to the radar by precipitation in the entire region behind the turbine (the spatial extent of which is typically on the order of several 100s of km$^2$). Figure 2.2 shows the effect of two wind turbines blocking a radar on

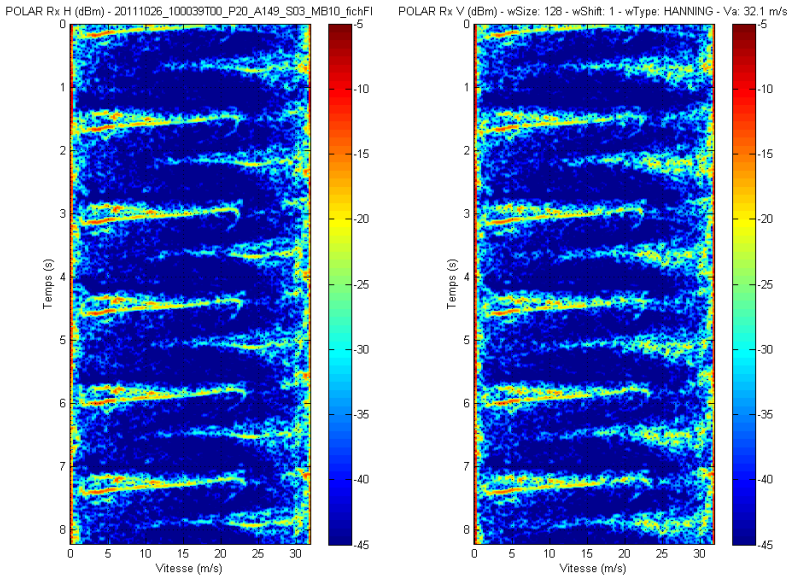


Figure 2.3: Example of Doppler spectra for a range gate with a wind turbine for horizontal (left) and vertical (right) polarization. These Doppler spectra are for the Abbeville (France) radar on 26-10-2011, 10:00 UTC, with Doppler velocity on the x-axis, time on the y-axis, and the colors indicating the power spectral density.

derived yearly rainfall accumulations. The severity of this effect is immediately clear from the figure, resulting in at least 10% local underestimates. It should be noted here that these accumulations are derived from a composite of two radars, where the composite reflectivity is a weighted mean of the two radars (and the weight depends on the distance to the radar). Furthermore, these data have been adjusted by rain gauges (see Overeem et al., 2008, for more details on this data set). Hence, despite the gauge correction and compositing with the second radar, at least 10% underestimation remains.

Because the amount of beam blockage is proportional to the physical cross-section of the turbine, the size and height of the turbine and its distance from the radar determine the severity of the problem, as illustrated in Figure 1.1. The larger the turbine, the more beam blockage. And it generally holds that turbines closer to the radar cause more blockage. It is therefore important to prevent wind turbines from being so close to the radar that they block a significant part of the main beam.

## 2.2 Impact on Doppler measurements

Wind turbines can have a significant impact on Doppler measurements. It has been shown that the entire Doppler spectrum is affected by wind turbines (e.g. Isom et al., 2009; Hood et al., 2010; OPERA, 2010). And hence also the moments

of the Doppler spectrum that are generally used (radial velocity $v_r$ and spectral width $\sigma_v$) are also heavily affected. This effect is shown in Fig. 2.3, which shows the time evolution of the Doppler spectrum of a radar measurement volume with a wind turbine (with the radar antenna stationary and pointed at the wind turbine). Because both radial velocity and spectral width are reflectivity-weighted moments (first moment and second central moment) of the radial velocity, the degree to which radial velocity moments are affected by wind turbine clutter depends on the clutter-to-signal ratio. So the effect on the Doppler moments is significant if the reflectivity caused by the wind turbines is of the same order of magnitude or greater than that of the weather.

Typical radar antenna rotation speeds are 1-8 rpm, resulting in a dwell time on any 1-degree measurement volume between 0.17 s and 0.02 s. So it is clear from Fig. 2.3 that the apparent mean Doppler velocity can be any value between $\sim -20$ m s$^{-1}$ and $\sim 20$ m s$^{-1}$, depending on the moment in time the wind turbine is sampled. It is likely, however, that the possible values that mean Doppler velocities from wind turbines will depend on the orientation of their blades with respect to the radar (see e.g. Fig. 1.1), and the angular velocity of the blades. The instantaneous effect of a wind turbine on mean Doppler velocity and spectral width is hence highly unpredictable. Note that in the example shown in Fig. 2.3 the Doppler spectra were recorded using a static antenna (unlike in an operational setting).

Norin (2015) shows a clear impact on Doppler data (both radial velocity and spectral width) of wind turbines. Clutter tails are also shown for these Doppler data. Hence, when the reflectivity exhibits clutter tails, these are also likely to be present in the Doppler data. The impact on long-term average mean Doppler velocity was shown (Norin, 2015) to be $\sim \pm 2.5$ m s$^{-1}$, and $\sim \pm 0.3$ m s$^{-1}$ for spectral width. Note that these are not instantaneous values but long-term averages, and that hence the underlying instantaneous values can greatly exceed these ranges.

## 2.3 Impact on dual-pol measurements

Dual-polarization radar variables ($\rho_{\mathrm{HV}}$, $Z_{\mathrm{DR}}$, LDR, and $\Phi_{\mathrm{DP}}$ or $k_{\mathrm{DP}}$) are based on both the amplitude and the phase of the returned radar signals (as are the reflectivity (see Section 2.1) and radial velocity (see Section 2.2)), and hence these variables are also affected by wind turbines. So, just like for reflectivity and Doppler variables, the effect on the dual-polarization moments is significant if the reflectivity caused by the wind turbines is of the same order of magnitude or greater than that of the weather. This effect has been clearly demonstrated by Hall et al. (2017). The use of dual-polarization radar variables for meteorological applications in the presence of wind turbines is hence limited. On the other hand, these variables offer potential for detection of wind turbine clutter, which can be used to filter data.

# Chapter 3

# Strategies to reduce the impact

The impact of wind turbines on weather radar data can be reduced at two stages in the radar processing chain: locally on the signal processor, or centrally on the radar product processor. For the purpose of impact reduction, the main difference between these two stages is that raw I/Q data are available on the signal processor and not on the product processor. This means that spectral analysis methods (e.g. Doppler filtering) can only be used on the signal processor. The main advantage of such spectral techniques is that for a given pixel the contribution to the total received power of weather can potentially be separated from that received from non-meteorological scatterers. Hence, a valid measurement is available for each pixel. Conversely, with post-processing on the product processor, an attempt can be made to identify pixels affected by wind turbines. The data from these pixels can subsequently be removed and filled in by using data from a different scan or by horizontal interpolation. Note that interpolation or filling of these removed areas reduces the quality of the data compared to a situation where there was no disturbance. This reduction becomes more severe as the area that is removed becomes larger.

## 3.1 Signal processing

Because wind turbine blades move when the wind turbine is turned on, standard Doppler ground clutter filtering will only be effective in removing the echoes from the turbine mast, but not from the blades. This is because Doppler ground clutter filters remove the part of the returned power from scatterers that have zero radial velocity. They hence assume ground clutter to be stationary, which the blades of the wind turbines are not. Hence, these filters are generally very effective when wind turbines are turned off (i.e., the blades don't rotate), and a large amount of clutter remains if the wind turbine is turned on (with moving blades). However, because for many wind turbines the reflectivity values are generally much higher than what is typically observed in precipitation, even if a wind turbine is turned off, the resulting value will be discarded. This is because of a thresholding mechanism that is generally applied in weather radars that discards any reflections with an excessive clutter-to-signal ratio. This threshold

is applied because with a finite number of pulses, a small part of the clutter power may leak to higher-velocity areas of the Doppler spectrum, which could lead to severe overestimates in case of a high clutter-to-signal ratio.

Recent research on using I/Q data for identification and filtering of wind-turbine affected radar pixels has shown some promising results, as well as limitations of the methods that were used. Norin (2017) has shown that it is possible to filter out disturbances caused by single wind turbines. This technique first detects wind turbine disturbances by searching for matches between the range profiles of I/Q data (with a resolution of 7.8 m) and typical range profiles of point targets (such as wind turbines). The areas that are identified as affected by wind turbines are subsequently removed and filled in by spatially interpolating both the amplitude and the phase gradient (so both reflectivity and radial velocity are realistic). This technique relies on the fact that individual wind turbines are separated in space by more than the effective length of the radar pulse ($\sim$ 150 m for a 0.5 $\mu$s pulse to $\sim$ 600 m for a 2.0 $\mu$s pulse in Norin, 2017). That means that this technique will not work for wind turbines that are part of wind parks, especially at longer pulse lengths. These longer pulse lengths are typically used operationally for low-level scans for maximum sensitivity, and unfortunately it is these low-level scans that are most affected by wind turbines. It should also be noted that this technique has only been tested on one month of data from one radar in Sweden, so it is not yet ready for operational implementation. Furthermore, it is not clear how this would work on radars across Europe with varying scan and signal processing settings. The spatial interpolation used in this technique will cause loss of data quality with respect to an undisturbed situation that needs to be taken into account as well.

Hood et al. (2010) present a method for detecting wind turbine contamination by combining several features of radar power spectra. These features (Clutter Phase Alignment, Spectral Flatness, $4^{\text{th}}$ central moment of the power spectrum, and Hub-to-Weather Ratio) are then combined in a fuzzy logic scheme. This technique has only been tested on a very limited dataset from a single S-band radar. Hood et al. (2010) also remark that their method may not work as well if there are multiple wind turbines in a single radar measurement volume. Note that this technique does not filter out wind turbine clutter, but only yields detections of wind-turbine-affected radar pixels.

Isom et al. (2009) show that a technique based on spectral spatial interpolation may be effective replacing the values of affected radar pixels. This technique spatially interpolates each spectral component of the Doppler spectrum so that all moments can be reconstructed. However, the performance of this technique was not better than that of simply spatially interpolating the radar moments (reflectivity and radial velocity; discussed in Section 3.2).

With polarimetric radars, using spectral polarimetry (Unal and Moisseev, 2004; Unal, 2009) for identification and filtering of wind turbine clutter may be a promising technique. This technique uses spectra of polarimetric variables to separate weather from other signals. However, this technique has not been tested on wind turbines, and has not yet been applied to operational radars. So it is too early to draw conclusions about the effectiveness of this technique for removing the effects of wind turbines from radar data.

While there has been research on removing the effect of wind turbines from weather radar data on the signal processor, the techniques have serious limitations and have not been fully tested on a range of operational radars. Fur-

thermore, it is unclear how well these techniques would work with the clutter tails caused by three-body scattering (see Fig. 2.1). However, it is important to keep following and supporting this type of research, because the techniques are certainly promising and may yield very valuable operationally implementable algoritms in the future.

## 3.2 Postprocessing

Post processing algorithms operate on data that are received from the signal processor. The only way that postprocessing algorithms can be used to remove the effect of wind turbines from the data is to remove the value of an affected pixel and attempt to find a substitute value. This substitution is often based on spatial (and sometimes temporal) interpolation (Isom et al., 2009). If interpolation is used, it is suggested that not only the spatial dimension is used, but also the temporal dimension. This means that the information from outside the area affected by wind turbines should be advected into this region, much like the temporal interpolation described by Fabry et al. (1994). It should be noted that this degrades the quality of the resulting data compared to an undisturbed situation, and that this degradation depends on the spatial extent of the area that is removed, as well as on the scales of spatial variation of the precipitation field. The larger the spatial extent of the area removed and the higher the spatial variation of the precipitation field, the lower the data quality, even if space-time interpolation methods are used. This is especially severe in the case of small-scale extreme precipitation, for which Bowler et al. (2006) have shown that temporal correlations are very small, so that even space-time interpolation methods will yield greatly decreased quality. For small-scale precipitation extremes, the removal of even a few $km^2$ of data would hence result in a significant decrease in the observed extreme.

An alternative to substituting the value of a given radar pixel by e.g. an interpolated value is simply not to use the data from that pixel in subsequent applications. Assimilation of weather radar data into Numerical Weather Prediction (NWP) models generally cannot use all of the radar data available, and a data thinning technique (e.g. Salonen et al., 2009) is often used before assimilation. Information about pixels affected by wind turbines can readily be used in such thinning techniques. It should be noted, however, that the extent of the area that is not usable should no exceed the typical scale of rain storms, because it is important for NWP to be able to assimilate these storms.

One of the advantages of clutter by wind turbines is that their location is known, so that localized filtering can be applied. Care should be taken, however, because propagation of the radar signal is affected by variations in humidity, temperature, and pressure (particularly vertical gradients, e.g. Steiner and Smith, 2002). The result of this is that under some conditions, the apparent locations of the wind turbines may shift, and a very different part of the beam will hit the wind turbine, potentially causing a much lower or higher reflection than under normal conditions (Hood et al., 2010). And the amount of clutter remaining after signal processing depends highly on whether the wind turbine is turned on (see Section 3.1). For proper identification of wind turbine clutter it is therefore important to have automated algorithms in place. This would ensure that data is not removed when the propagation conditions are such that no wind

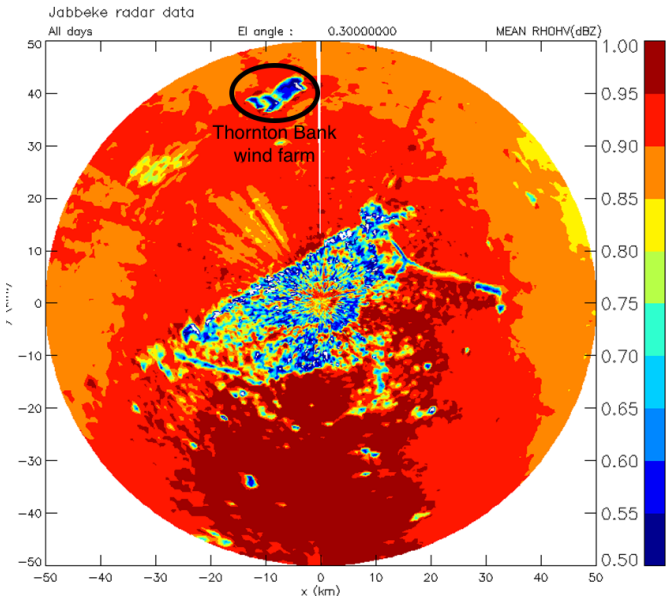


Figure 3.1: Copolar correlation coefficient ($\rho_{\mathrm{HV}}$) from lowest PPI (0.3°) for the Jabbeke radar (BE) averaged over 6 rainy days. Wind turbines from Thornton Bank 40 km to the north of the radar produce a very clear signature on $\rho_{\mathrm{HV}}$ data. Ground clutter also produces a clear signal in $\rho_{\mathrm{HV}}$.

turbine clutter is present, or if the wind turbine is switched off. Conversely, it will help in improving data quality when wind turbine clutter is present due to e.g. extreme propagation conditions.

Hood et al. (2010) present an effective method to detect radar pixels affected by wind turbines (see also Section 3.1). Such methods can nicely be complemented by using polarimetric variables. For example, Fig. 3.1 shows the co-polar correlation coefficient $\rho_{HV}$ averaged over 6 rainy days for the Jabbeke radar in Belgium. The wind turbines $\sim$ 40 km from the radar show very clear $\rho_{HV}$ signatures. This demonstrates the potential of using $\rho_{HV}$ for detecting wind turbines. Keränen et al. (2014) and Hall et al. (2017) have shown that the use of polarimetric variables is indeed effective for the detection of wind turbine disturbance of weather radar signals.

As mentioned above, once detected, wind turbine clutter can only be removed from the data by either blanking these data or by interpolating. And the quality of the resulting data greatly depends on the extent of the wind turbine clutter and the scale of spatial variation of precipitation. Typical spatial scales of variation of precipitation vary with climate and with season. van de Beek et al. (2012) showed that typical scales of variation of 5-minute accumulations of precipitation in the Netherlands are on the order of $\sim$ 30 km in winter and $\sim$ 17 km in summer. It should be noted here that these scales are distances over which precipitation has completely decorrelated, so in order to still be able to capture some of the features of the underlying precipitation field, disturbances should be much smaller than these scales. Similar studies in Southern France yield typical spatial scales of 5-minute accumulations of precipitation of $\sim$ 12 km

(Lebel et al., 1987) and $\sim$ 10 km (Berne et al., 2004). This means that the spatial extent of wind turbine disturbances of radar data should not exceed these scales in order to avoid the radar completely missing the most intense part of a rainfall event.

For correction for beam blocking by wind turbines, the movement of the wind turbine blades and the variation of the orientation of the hub with wind direction causes the magnitude of this blockage to be both variable and unpredictable. This makes it very difficult to correct for this loss of power. However, the part of the beam blocked by the tower and part of the hub does cause a constant attenuation, and hence could potentially be corrected for. This does require that the amount of blocking by this wind turbine mast, which is difficult to estimate, is known. Because the effect of beam blocking can be severe, as is shown in Fig. 2.2, the beam blockage caused by wind turbines should be limited to approximately 0.5 dB (i.e., approximately 10% in terms of returned power and 7.5% in terms of rainfall estimates if the $Z - R$ relation by Marshall et al. (1955) is used).

Correction of radar data by rain gauges is often applied for hydrological use (e.g. Goudenhoofdt and Delobbe, 2009). However, this will likely not lead to proper correction for beam blockage by wind turbines because it is unlikely that a gauge is in the area being blocked (see also Fig. 2.2). If there is a gauge in this area, the resulting correction will likely deteriorate the quality of the final precipitation estimate because of the spatially smooth nature of these correction techniques. The area affected by the beam blockage will likely be properly corrected (at least close to the rain gauge), but the area not affected by beam blockage will likely be overcorrected. It is therefore very important to limit this underestimation.

# Chapter 4

# Impact of wind turbine disturbance on end users of radar data

It is important to understand the potential impact of wind turbines on end users of weather radar data, particularly where public safety is concerned. This impact on end users is discussed in this chapter and is based on scientific literature. From this, the effect of the spatial extent and the strength of wind turbine clutter on warnings for extreme weather, hydrological applications, climate monitoring, hail detection, and assimilation into numerical weather prediction models can be quantified.

For hydrological applications, the effect of wind turbine clutter in radar data can be very large if the wind turbine clutter is accumulated over long time periods. This leads to large apparent accumulations of precipitation at the wind turbine location, leading to false warnings for floods. In most cases, these warnings will be ignored by operators of flood control systems because the warning is not consistent with the weather that the operators observe themselves. However, this does decrease the credibility of such flood warning systems, potentially leading to not heeding the warning in case of real precipitation. However, the biggest effect will be on automated warning systems (e.g. LAPS; see Gregow et al., 2017), as no human intervention is designed into the system.

If it is assumed that the influence of the wind turbines is corrected for, such false warnings will generally not occur. Interpolation or advection of radar data from around the wind turbine location will yield more realistic precipitation estimates, leading to much more accurate warnings. This will hold if the size of the area affected by the wind turbines is smaller than the typical size of rain events. If a convective storm (generally intense and small-scale) passes over an affected area that is larger than the storm, the storm can be missed by the radar, resulting in a failure to warn for extreme precipitation. The most devastating floods occur as a result of local convective storms that are nearly stationary (Delrieu et al., 2005). Hence, advection of data into the affected area would not help here. Such a failure to warn for extreme precipitation can lead to loss of property and loss of lives. As shown in Section 3.2, typical scales of convective storms are on the order of 10 km. Wind farms with spatial extents exceeding

this scale are hence most likely to cause such problems.

For the derivation of climatologies of extreme rainfall, a similar effect can be expected: if the area affected by wind turbines is larger than the typical scale of storms, the most extreme accumulation of precipitation can be missed. This can lead to underestimates of the extremes that can occur. These estimates of extremes are subsequently used for dimensioning of drainage systems or flood protection systems such as dykes. It should be noted here that missing a single event will not have a very large effect on the derived statistics, given the uncertainty estimates that accompany these statistics. On the other hand, extreme precipitation is generally caused by small-scale (i.e., approximately 10 km) precipitation systems, especially when considering the short-duration extremes that generally cause urban flooding (e.g. Smith et al., 2001, 2005).

Weather forecasting and providing warnings about heavy precipitation for the general public will also be affected by wind turbine clutter. This may happen in several ways. When the size of the area affected by wind turbine clutter is smaller than typical storm scales, most forecasters can recognize the cluttered area for what it is, and will not issue any false warnings. On the other hand, if a storm were to develop over such an area, its size would soon exceed the size of the cluttered area, and would become apparent to the forecaster. The fact that a forecaster typically also has access to geostationary satellite information about cloud tops helps with this. However, when the size of the affected area exceeds the typical size of storms, the forecaster is likely to miss the initial stages of the storm, which can cause costly delays in issuing warnings. It should be noted that the above holds for warnings that are based on systems that include human interventions. Fully automated systems will suffer more from the effects of wind turbines on radar data.

If a storm is over a wind turbine location, the respective signals form the turbine and the rain are added. If the reflections from the turbine dominate those from the storm, the received signal characteristics will be those of a turbine and the data will likely be labelled as such by any wind turbine detection algorithm. Hence, in case of no rain or rain lighter than the wind-turbine equivalent, the radar data from that point will be removed and interpolated. Conversely, if the reflections from the storm are much larger than those from a turbine, signal characteristics will be like those of rain and will not be detected by a wind turbine detection algorithm. This is not a problem in this case, as the overestimation due to the wind turbine contribution to the signal power will be negligible. Hence, it is advisable to only pose restrictions to wind turbine development if the expected reflections from these turbines exceed reflectivities typical for disruptive weather.

So end users are affected by wind turbine disturbances in radar data if the reflectivity is above a certain threshold, and if the spatial extent of the disturbances is larger than typical storm sizes. It is well-known that summer-time convection can be both disruptive and small-scale. However, it should be noted here that it is not only necessary to provide warnings for summer-time convective storms, but also for winter-time snow. Convective snow storms in the winter have typical scales that are similar to summer-time convective storms. However, their peak reflectivity can be much lower, on the order of 20 dBZ (e.g. Huang et al., 2010), and these storms are generally generated over sea and advected over land. This and the fact that their internal dynamics are less severe results in less quality loss when space-time interpolation is used.

Radars are not only used to warn for heavy precipitation, but also for phenomena associated with intense summer-time convection, such as downbursts, tornadoes and severe hail. The scales of such phenomena are generally even smaller than typical scales of precipitation systems, and their reflectivities are much higher. Seltmann and Böhme (2017) have shown the effect of wind turbines on the automated generation of such warnings, even for small wind farms. Hence, these small-scale and high-intensity phenomena should be treated separately. Criteria for automated detection of severe convection are described by Seltmann and Böhme (2017) to be at least 15 contiguous $1 \times 1$-km$^2$ pixels exceeding 46 dBZ (corresponding to a rainfall intensity of approximately 30 mm h$^{-1}$ when using the $Z - R$ relation by Marshall et al. (1955)). In order to limit the probability that a storm of only a few pixels will generate a warning, very-high-intensity wind turbine clutter over a contiguous area of 15 km$^2$ should be avoided.

A more indirect effect that wind turbine clutter can have on forecasting weather (including providing warnings) is that radar data are assimilated into Numerical Weather Prediction (NWP) models. Hence, if not properly detected, wind turbine clutter can potentially influence the NWP output. However, it is known that most data assimilation schemes actually reject radar observations that are very far from the model state, thereby limiting the effect of the disturbances in radar reflectivity. This is likely different for radial velocities, however, so the effect can certainly have a larger impact there. If properly detected, pixels (of both reflectivity and radial velocity) with wind turbine clutter can safely be removed from the data so that they will not be assimilated into NWP models.

Hail monitoring with non-polarimetric radars is based on detecting the height of the echo tops (Holleman et al., 2000), and is only used to detect summer-time hail. The probability of hail is determined from the echo top height above the 0°C isotherm. This means that in order for wind turbine clutter to affect hail monitoring, it must be present in higher elevation scans. In order for this to happen under normal propagation conditions, a wind turbine should either extend into these higher beams, or the sidelobe reflections of the wind turbines should be very large. This generally only happens if the wind turbine is very close to the radar. However, this does not hold in anomalous propagation conditions, resulting in erroneous high probabilities of hail. Proper real-time detection of wind turbine clutter in weather radar data is necessary to solve this problem.

The effect of beam blockage on end users of weather radar data depends on its severity. Hydrological applications will suffer most from the loss of power behind a wind turbine. The resulting underestimate of rainfall intensities in a line behind the wind turbine (see Fig. 2.2) will lead to underestimates of recharge of ground water levels and flood peaks. If it is desired to limit the underestimate in rainfall accumulation to a maximum of 7.5%, the maximum power loss caused by beam blockage by wind turbines should not exceed 10% (i.e. $\sim 0.5$ dB), using a standard relation for computing rainfall intensities from radar reflectivity factors (i.e., the Marshall-Palmer relation, see Marshall et al., 1955). For other applications the beam blockage needs to be larger in order for the end users to be significantly affected (i.e. threshold exceedance for severe storm warning could potentially not occur due to beam blockage). This is generally not the case unless the turbine is very close to the radar (and in its main beam).

# Chapter 5

# Conclusions and recommendations

## 5.1 Conclusions

Wind turbines can have significant influence on weather radar measurements. The fact that wind turbines have moving blades with variable orientation and velocities make this effect both highly unpredictable and difficult to correct for. Furthermore, the fact that wind turbines reflect radio waves very efficiently results in potentially very strong reflections, especially if they are close to the radar and reach into the main lobe. This becomes more severe under anomalous propagation conditions when also wind turbines much further away can cause very intense reflections. If radar reflectivity values are affected by wind turbines, radial velocity and dual-polarization variables in corresponding pixels will also be affected. If convective snow should be detected, wind turbine clutter above 20 dBZ should be avoided over areas exceeding a typical scale of 10 km. Because severe summertime convective storms have more intense internal dynamics and are typically generated over land, these values change to 46 dBZ and 4 km (corresponding to an area of 15 $km^2$).

Algorithms for correcting wind turbine reflections on the radar signal processor have not (yet) been proven to be effective. Research into new signal-processor algorithms for *detecting* wind turbine echoes yield promising results. However, these algorithms are typically not mature enough yet for operational implementation. Post-processing algorithms have been shown to be effective in detecting pixels affected by wind turbines in several case studies, especially when combined with polarimetric variables. There are, however, no studies showing the effectiveness of these algorithms over a large number of radars. Furthermore, there are no dedicated wind-turbine detection algorithms available on any radar system.

Substitution algorithms for replacing wind-turbine-affected pixels are generally based on spatial or temporal interpolation. The effectivity of these algorithms hence depends on the size of the area that is disturbed by wind turbines, and the typical space-time extent of storms. The resulting maximum spatial extent of wind turbine disturbances is 10 km. However, these algorithms will always cause degradation of data quality with respect to an undisturbed situa-

tion, even if the most advances space-time interpolation methods are used. It should also be noted that both automated detection and substitution algorithms are not currently operationally available. This means that dealing with wind turbine clutter relies heavily on the ability of human forecasters to recognize this type of clutter. And if such algorithms are available for a given radar, the quality of the resulting data greatly depends on the ability of these algorithms to properly detect and mitigate the effects of wind turbines.

## 5.2 Recommendations

It is clear that wind turbines affect weather radar data, even very far from the radar (beyond 100 km). Having guidelines about where to place wind turbines with respect to weather radars will certainly help to avoid significant disturbances of radar data: a wind turbine will not affect radar data if it is not there (or if there is no free line of sight). Because most governments in Europe are actively stimulating wind energy, it is unrealistic and unwanted to try to block all wind turbine development that may affect radar data quality. It is therefore very important to have a set of objective criteria against which wind turbine applications can be judged. It is recommended that such international guidelines are drafted, preferably in close collaboration with WMO. Such guidelines should be evaluated and updated on a regular basis. Current guidelines (OPERA, 2010; WMO, 2010) should be used until new guidelines are in place.

Besides drafting new guidelines, it is recommended to keep following the developments in data processing techniques. Facilitating and participating in studies that focus on development and testing of new techniques will help accelerate these developments. Furthermore, it is necessary to empirically quantify the effect of wind turbine clutter on dual-polarization variables.

It is also recommended that wind turbine developers take the position of weather radars into account when planning wind parks, and to explore the use of non-reflective ('stealth') materials in wind turbines. Weather radar operators should take the position of existing and planned wind turbines into account when seeking a site for placement of a weather radar.

In short, it is recommended to

- use current guidelines (OPERA, 2010; WMO, 2010) until new international guidelines with respect to the placement of wind turbines are in place;
- draft new international guidelines with respect to the placement of wind turbines in close collaboration with WMO;
- re-evaluate these guidelines regularly in order to keep up with developments e.g. regarding radar filtering;
- follow literature regarding the development of filters for separating wind turbine and meteorological power in each measurement volume;
- study the effect of wind turbines on polarimetric variables (e.g., $Z_{DR}$, $\Phi_{DP}$, $\rho_{HV}$);
- participate in development of data processing methods that minimize the effect of the wind turbines on the weather service;

- for wind turbine developers to take the location of weather radars into account when planning the placement of wind turbines;
- for wind turbine developers to consider using stealth materials in wind turbines.

# Bibliography


Angulo, I., O. Grande, D. Jenn, D. Guerra, and D. de la Vega, 2015: Estimating reflectivity values from wind turbines for analyzing the potential impact on weather radar services. *Atmos. Meas. Tech.*, **8**, 2183–2193, doi:10.5194/amt-8-2183-2015.

van de Beek, C. Z., H. Leijnse, P. J. J. F. Torfs, and R. Uijlenhoet, 2012: Seasonal semivariance of Dutch rainfall at hourly to daily scales. *Adv. Water Resour.*, **45**, 76–85, doi:10.1016/j.advwatres.2012.03.023.

Berne, A., G. Delrieu, J.-D. Creutin, and C. Obled, 2004: Temporal and spatial resolution of rainfall measurements required for urban hydrology. *J. Hydrol.*, **299**, 166–179.

Bowler, N. E., C. E. Pierce, and A. W. Seed, 2006: STEPS: A probabilistic precipitation forecasting scheme which merges an extrapolation nowcast with downscaled NWP. *Q. J. R. Meteorol. Soc.*, **132 (620)**, 2127–2155, doi:10.1256/qj.04.100.

Delrieu, G., and Coauthors, 2005: The catastrophic flash-flood event of 8-9 September 2002 in the Gard region, France: a first case study for the Cévennes-Vivarais Mediterranean Hydro-meteorological Observatory. *J. Hydrometeorol.*, **6 (1)**, 34–52, doi:10.1175/JHM-400.1.

Fabry, F., A. Bellon, M. R. Duncan, and G. L. Austin, 1994: High resolution rainfall measurements by radar for very small basins: the sampling problem reexamined. *J. Hydrol.*, **161**, 415–428.

Goudenhoofdt, E., and L. Delobbe, 2009: Evaluation of radar-gauge merging methods for quantitative precipitation estimates. *Hydrol. Earth Sys. Sci.*, **13**, 195–203, doi:10.5194/hess-13-195-2009.

Gregow, A., E. Pessi, A. Mäkelä, and E. Saltikoff, 2017: Improving the precipitation accumulation analysis using lightning measurements and different integration periods. *Hydrol. Earth Sys. Sci.*, **21**, 267–279, doi:10.5194/hess-21-267-2017.

Hall, W., M. A. Rico-Ramirez, and S. Krämer, 2017: Offshore wind turbine clutter characteristics and identification in operational c-band weather radar measurements. *Q. J. R. Meteorol. Soc.*, **143 (703)**, 720–730, doi:10.1002/qj.2959.

Holleman, I., H. R. A. Wessels, J. Onvlee, and B. S. J. M., 2000: Development of a hail-detection-product. *Phys. Chem. Earth*, **25**, 1293–1297, doi:10.1016/S1464-1909(00)00197-0.

Hood, K., S. Torres, and R. Palmer, 2010: Automatic detection of wind turbine clutter for weather radars. *J. Atmos. Oceanic Technol.*, **27**, 1868–1880, doi:10.1175/2010JTECHA1437.1.

Huang, G.-J., V. N. Bringi, R. Cifelli, D. Hudak, and W. A. Petersen, 2010: A methodology to derive radar reflectivityliquid equivalent snow rate relations using C-band radar and a 2D Video Disdrometer. *J. Atmos. Oceanic Technol.*, **27 (4)**, 637–651, doi:10.1175/2009JTECHA1284.1.

Isom, B. M., and Coauthors, 2009: Detailed observations of wind turbine clutter with scanning weather radars. *J. Atmos. Oceanic Technol.*, **26**, 894–910, doi:10.1175/2008JTECHA1136.1.

Keränen, R., L. C. Alku, A. Pettazzi, and S. Salsón, 2014: Weather radar and abundant wind farming – impacts on data quality and mitigation by Doppler dual-polarization. *Proceedings of the 8$^{\text{th}}$ European Conference on Radar in Meteorology and Hydrology*, Garmisch-Partenkirchen, Germany, 188, URL http://www.pa.op.dlr.de/erad2014/programme/ExtendedAbstracts/188_Keranen.pdf.

Krajewski, W. F., and J. A. Smith, 2002: Radar hydrology: rainfall estimation. *Adv. Water Resour.*, **25 (8-12)**, 1387–1394, doi:10.1016/S0309-1708(02)00062-3.

Lebel, T., G. Bastin, C. Obled, and J. D. Creutin, 1987: On the accuracy of areal rainfall estimation: A case study. *Water Resour. Res.*, **23 (11)**, 2123–2134, doi:10.1029/WR023i011p02123.

Marshall, J. S., W. Hitschfeld, and K. L. S. Gunn, 1955: Advances in radar weather. *Adv. Geophys.*, **2**, 1–56.

Maynard, R. H., 1945: Radar and weather. *J. Meteorol.*, **2**, 214–226, doi:10.1175/1520-0469(1945)002⟨0214:RAW⟩2.0.CO;2.

Norin, L., 2015: A quantitative analysis of the impact of wind turbines on operational doppler weather radar data. *Atmos. Meas. Tech.*, **8 (2)**, 593–609, doi:10.5194/amt-8-593-2015.

Norin, L., 2017: Wind turbine impact on operational weather radar I/Q data: characterisation and filtering. *Atmos. Meas. Tech.*, **10 (5)**, 1739–1753, doi:10.5194/amt-10-1739-2017.

Norin, L., and G. Haase, 2012: Doppler weather radars and wind turbines. *Doppler Radar Observations – Weather Radar, Wind Profiler, Ionospheric Radar, and Other Advanced Applications*, J. Bech, Ed., InTech, chap. 14, 333–354, doi:10.5772/39029.

OPERA, 2006: OPERA II work package 1.8: Impact of wind turbines on weather radars. Tech. Rep. OPERA_2006_18, OPERA.

OPERA, 2010: OPERA III work package 1.5b: Site protection (wind turbines). Tech. Rep. OPERA_2010_05, OPERA. URL http://eumetnet.eu/wp-content/uploads/2017/01/OPERA_2010_05_Wind_turbines-1.pdf.

Overeem, A., A. Buishand, and I. Holleman, 2008: Rainfall depth-duration-frequency curves and their uncertainties. *J. Hydrol.*, **348**, 124–134, doi:10.1016/j.hydrol.2007.09.044.

Overeem, A., I. Holleman, and A. Buishand, 2009: Derivation of a 10-year radar-based climatology of rainfall. *J. Appl. Meteorol. Clim.*, **48**, 1448–1463, doi:10.1175/2009JAMC1954.1.

Salonen, K., H. Järvinen, G. Haase, S. Niemelä, and R. Eresmaa, 2009: Doppler radar radial winds in HIRLAM. Part II: optimizing the super-observation processing. *Tellus A*, **61 (2)**, 288–295, doi:10.1111/j.1600-0870.2008.00381.x.

Seltmann, J. E. E., and T. Böhme, 2017: Wind turbine issues in Germany. *Proceedings of the 38$^{\text{th}}$ Conference on Radar Meteorology*, Chicago, American Meteorological Society, https://ams.confex.com/ams/38RADAR/meetingapp.cgi/Paper/320410.

Smith, J. A., M. L. Baeck, Y. Zhang, and C. A. Doswell Jr., 2001: Extreme rainfall and flooding from supercell thunderstorms. *J. Hydrometeorol.*, **2 (4)**, 469–489.

Smith, J. A., A. J. Miller, M. L. Baeck, P. A. Nelson, G. T. Fisher, and K. L. Meierdiercks, 2005: Extraordinary flood response of a small urban watershed to short-duration convective rainfall. *J. Hydrometeorol.*, **6**, 599–617.

Steiner, M., and J. A. Smith, 2002: Use of three-dimensional reflectivity structure for automated detection and removal of nonprecipitating echoes in radar data. *J. Atmos. Oceanic Technol.*, **19 (5)**, 673–686, doi:10.1175/1520-0426(2002)019⟨0673:UOTDRS⟩2.0.CO;2.

Sun, J., and Coauthors, 2014: Use of nwp for nowcasting convective precipitation: Recent progress and challenges. *Bull. Am. Meteorol. Soc.*, **95**, 409–426, doi:10.1175/BAMS-D-11-00263.1.

Unal, C. M. H., 2009: Spectral polarimetric radar clutter suppression to enhance atmospheric echoes. *J. Atmos. Oceanic Technol.*, **26**, 1781–1797, doi:10.1175/2009JTECHA1170.1.

Unal, C. M. H., and D. N. Moisseev, 2004: Combined Doppler and polarimetric radar measurements: correction for spectrum aliasing and nonsimultaneous polarimetric measurements. *J. Atmos. Oceanic Technol.*, **21**, 443–456, doi:10.1175/1520-0426(2004)021⟨0443:CDAPRM⟩2.0.CO;2.

Vogt, R. J., J. Reed, T. Crum, J. T. Snow, R. Palmer, B. Isom, and D. W. Burgess, 2007: Impacts of wind farms on WSR-88D operations and policy considerations. *23$^{\text{rd}}$ International Conference on Interactive Information and Processing Systems for Meteorology, Oceanography, and Hydrology*, San Antonio, TX, USA, American Meteorological Society, Paper 5B.7.

WMO, 2010: CIMO XV abridged final report of the commission for instruments and methods of observation, fifteenth session, with resolutions and recommendations. Tech. Rep. 1064, World Meteorological Organization. URL http://www.wmo.int/pages/prog/www/CIMO/CIMO15-WMO1064/1064_en.pdf.

# Appendix A

# Report on Investigations on the spatial extent of the effect of wind turbines on radar data

# Investigations on the spatial extent of the effect of wind turbines on radar data

Reinhard Teschl, Helmut Paulitsch, Franz Teschl

Graz University of Technology (TU Graz), Austria

In many European countries, the promotion of the use of renewable energy sources becomes apparent in the installation of new wind power stations and the repowering or expansion of existing wind farms. However, for weather radar service providers this trend gives cause for concern. As wind power stations are primarily installed at exposed locations, and their typical dimensions have increased over the years, they affect the propagation of radar signals and thus impact the data quality of weather radar stations.

EUMETNET OPERA has initiated studies to reassess its current guidelines towards wind turbines in the vicinity of weather radar stations for ensuring wind turbine free areas around radar sites. The present study makes a contribution to this effort by investigating the spatial extend of the effect of wind turbines on weather radar data.

The areas around two wind farms in the Netherlands that are surveilled by the radar site in Emden, Germany were investigated. As of the two-year period of investigation from November 2010 to October 2012, no other wind turbines were located between these wind farms and the weather radar site.

The general approach was to categorize the radar coordinates according to their relative location and distance to the coordinates of the wind farm. The coordinates in front, behind, and at the side (as seen from the radar) of the wind farms were analyzed separately. The mean reflectivity as well as the distribution of the measurements were investigated during different weather conditions.

First results indicate that especially coordinates separated laterally only by 1° seem to be influenced by wind turbines.

This draft is organized as follows: First, in the introduction, sources of misplaced echoes are described. Second, the coordinate selection is presented followed by a description of the applied methods. The results are given in the form of mean reflectivity- and exceedance probability maps and statistical figures.

Introduction

Wind turbines (WT) that extent into the main lobe of a weather radar usually reflect one fraction of the radar signal back to the radar. The WT-backscatter interferes with the meteorological echoes from precipitation at that range gate. As a consequence, the desired meteorological echo (precipitation) is superimposed by the non-meteorological echo (wind turbine). But not only the range gate (radar coordinate) where the WT is situated, might be affected. The antenna does not only collect information from the main lobe, which typically has a half power beam width of 1°. Also higher angles where the power has fallen below half (-3 dB) of its maximum value, and the distinct side lobes have to be considered. Wind turbines in the vicinity of a radar can exhibit backscatter in such an order of magnitude, that they are also detected via the side lobes. Because of this side lobe, also objects (with high backscatter) that are not in the focus of the radar can lead to significant yet incorrectly placed echoes (Figure 1). Thus, a wind farm may cause echoes beyond its geographic position and thus effects radar data beyond its actual range gate.

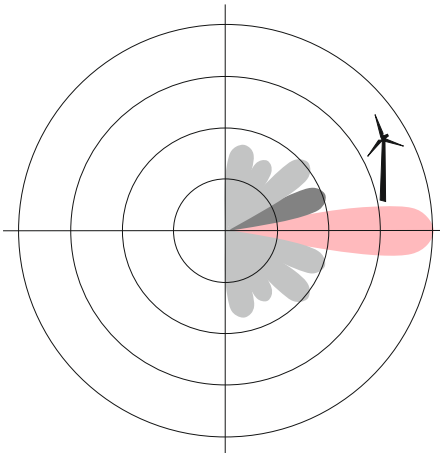

**Figure 1: Schematic illustration of a wind turbine that is detected by a side lobe of the radar antenna (Annotation: The back lobe and side lobes beyond +/- 90° from the main lobe are not depicted).**

Moreover, it is not only possible that the echo is misplaced azimuthally. If the constellation (in terms of geometry and scattering angle) fits, it is also conceivable that echoes of wind turbines appear farther away. Namely, when the radar beam is not only directly reflected back, but by another body. A known phenomenon in this respect are hail spikes. Hail spikes result when the radar beam is reflected by a volume of hail to the ground and then back to the hail. If the radar beam finds its way from there back to the radar antenna, it appears on the radar display as a spike of weak echoes with the same azimuth angle as the hail volume, but due to the longer travel time of the radar waves, with higher range.

Such multiple scattering scenarios are also possible with wind farms, provided an occasion in terms of arrangement of radar, windfarm, and orography (see Figure 2).

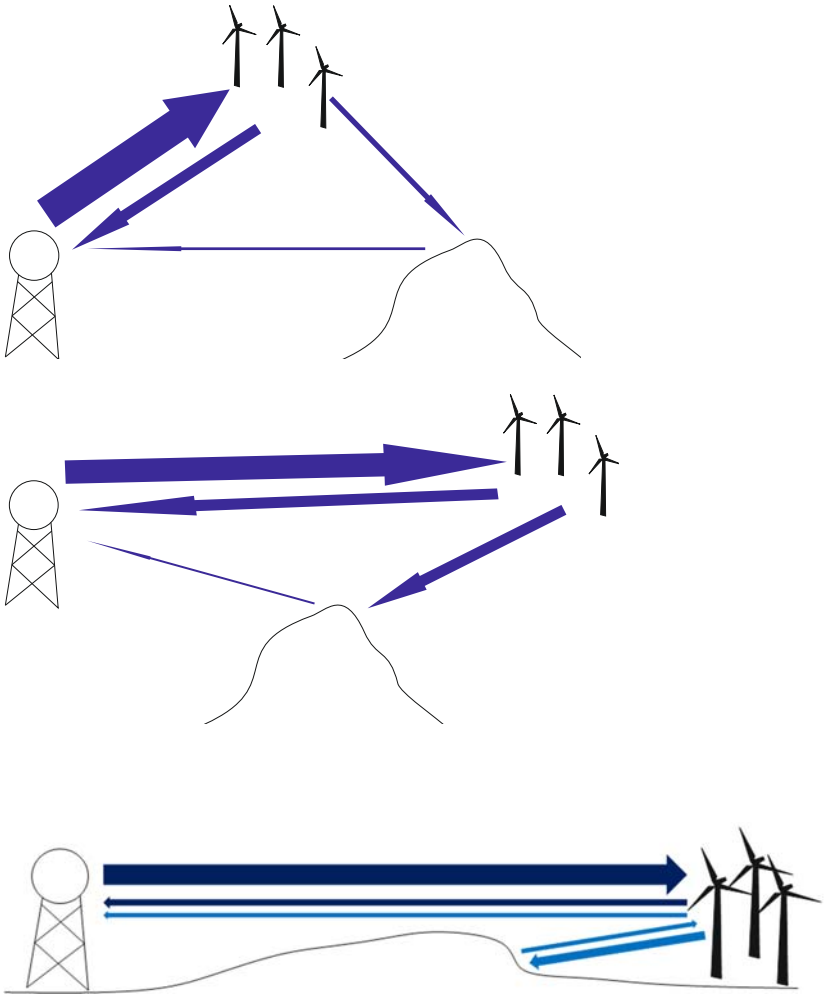

**Figure 2: Illustration of multiple body scattering.**

The consideration above drafts a scenario where an echo occurs behind the wind farm (from the perspective of the radar) because of the presence of the wind farm. However, wind farms may also act as obstacles, shielding parts of the radar beam and thus leading to an underestimation of the true reflectivity in the range gates behind them.

## Study area and coordinate selection

In view of the examples and scenarios depicted above, the selection of the study area and the coordinates for the statistical analyses was made. Two wind farms in the Netherlands were chosen for this study. One wind farm is located near Delfzijl, the other at Eemshaven. Both areas are surveilled with good visibility by the German weather radar in Emden. See Figure 3 for a map of the whole study area.

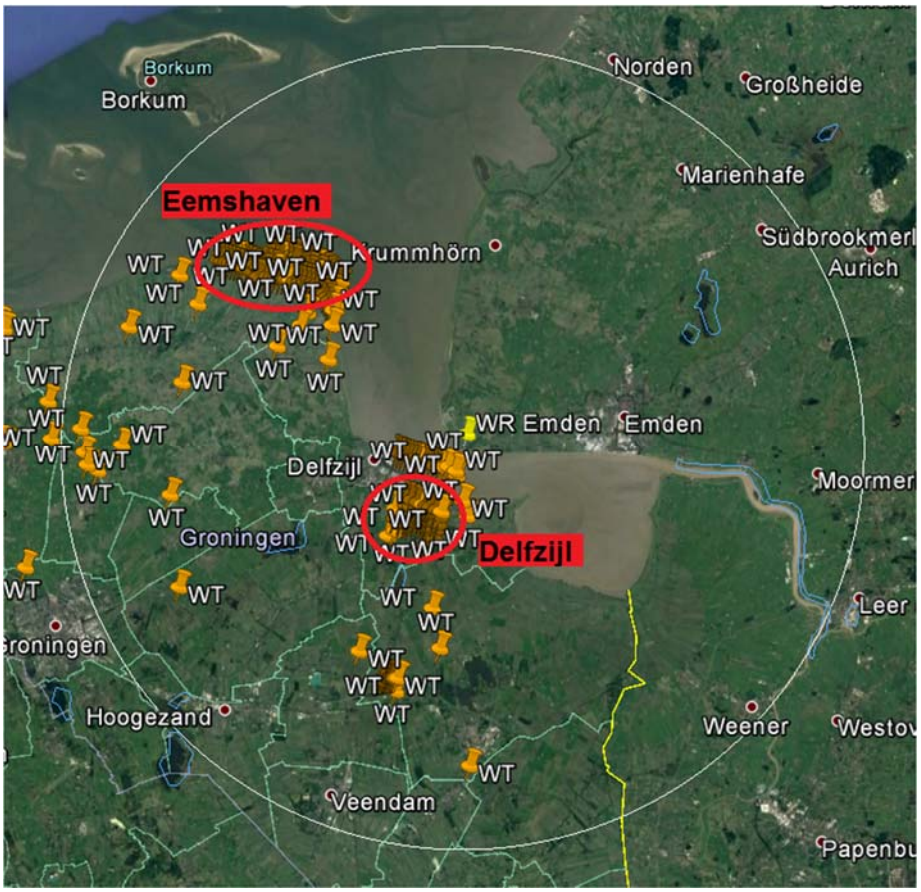


**Figure 3: The location of the two selected wind farms in the Netherlands with respect to the weather radar in Emden, Germany. The wind farm near Delfzijl is located to the south-west of Emden [Annotation: the wind turbines (WT) between this wind farm and the radar site did not exist during the two-year period of investigation]. The wind farm at Eemshaven is situated northwestern of Emden (Map: Google Earth).**

The coordinates chosen for the statistical analysis are situated in front, behind, and to the side of the wind farm (as seen from the radar). The scenarios in the introduction indicate that effects of a wind turbine on the radar coordinates behind and to the sides are conceivable. The coordinates in front are not believed to be influenced by wind turbines behind. Thus, only wind farms were chosen with no other turbines between them and the radar (during the period of investigation between November 2010 and October 2012).

Figure 4 and Figure 5 show the coordinates in front, behind and to the side of the wind farms near Delfzijl and Eemshaven that were selected. The spatial extent of wind farms may lead to constellations where a coordinate e.g. in front of a wind turbine is at the same time to the side of another wind turbine. As the front coordinates are seen as a reference, only such coordinates are termed “in front” that are not to the side (up to 4°) of another coordinate comprising a wind turbine. This is the reason, why at Eemshaven only two coordinates are identified as in front (Annotation: Coordinates of wind turbines not belonging to the wind farm are not shown).

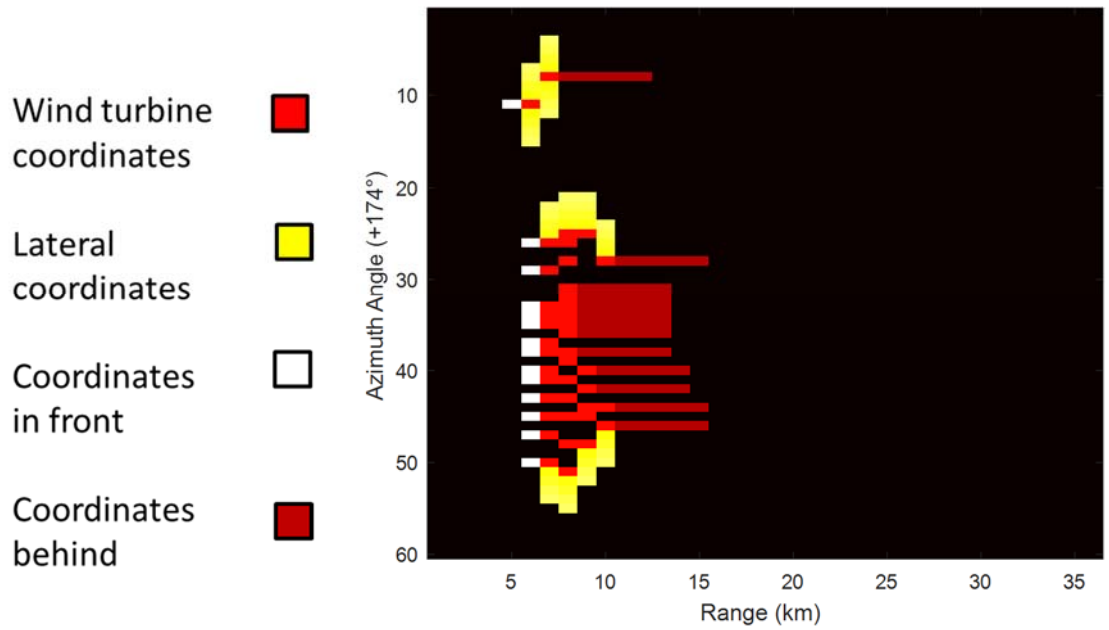


**Figure 4: Selected coordinates in front, behind and to the side of the wind farm near Delfzijl**

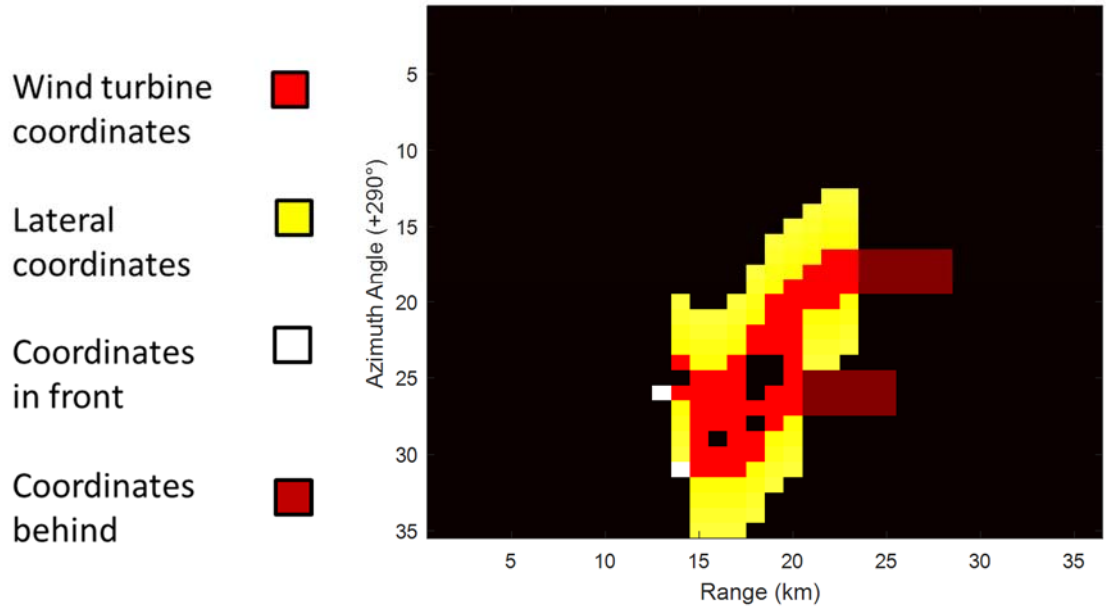


**Figure 5: Selected coordinates in front, behind and to the side of the wind farm near Eemshaven**

Methodology

In order to depict the spatial extent of the influence of wind turbines, two forms of representation were chosen. First, visual representations, namely maps, showing the mean reflectivity and other measures of the area around the depicted wind farms. Second, in the form of statistical measures and curves. Below these forms of representation are described in more detail.

Reflectivity maps

These maps show the mean reflectivity of the study area. Radar coordinates that comprise wind turbines that extent into the radar beam, generally show persistent echoes. As a consequence the mean reflectivity (calculated over the whole period of investigation or over specific weather situations) is high.

Exceedance probability maps

Due to multiple scattering scenarios echoes, radar coordinates in the vicinity of the wind turbine may show echoes only sporadically yet more often than at coordinates farther away from the wind turbine. Such patterns may not be visible in averaged reflectivity maps. Therefore, in addition maps depicting the probability of exceedance of certain reflectivity thresholds are shown.

Statistical analysis

The statistical approach will quantitatively summarize the information in the maps. It will be based on a frequency analysis of the measurements at power station sites, compared to sites in the vicinity without these buildings. The empirical cumulative distribution function (CDF) will be applied to reveal the differences between the measurements at different sites (see Figure 6). The bootstrap analysis simulates a different selection of coordinates and the possible variation of the mean values (Figure 7). New datasets of the same size are generated by „sampling with replacement“ from the original dataset (using 10 000 Bootstrap-samples each).

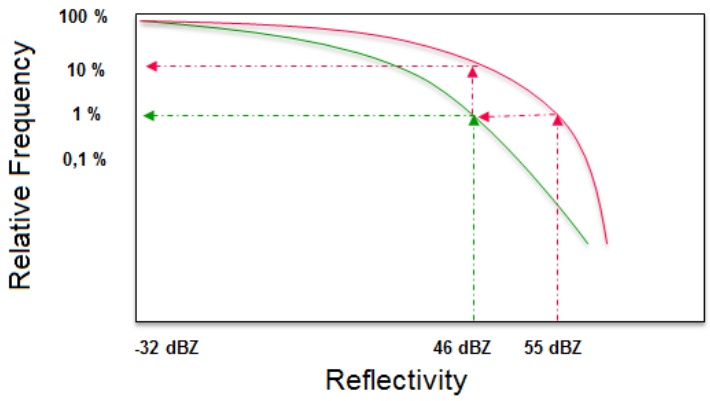


**Figure 6: Schematic representation of the empirical cumulative distribution function (CDF) in the inverse form. It shows the relative frequency of occurrence of values greater or equal to the value on the abscissa.**

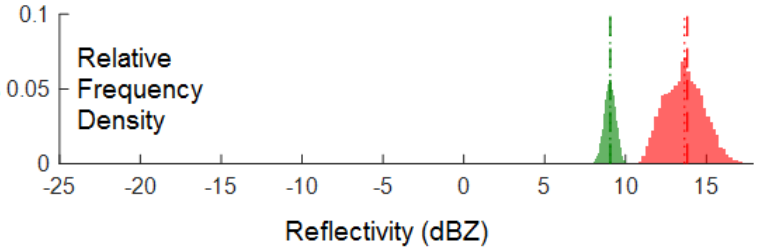


**Figure 7: Frequency distribution of mean values. Bootstrap Analysis (Re-sampling) simulates a different selection of coordinates and the possible variation of the mean values.**

Available data

The analysis is based on the polar radar reflectivity product labelled DX. DX has an operating range of 128 km with a range resolution of 1 km and an angular resolution of 1°. The product is updated every 5 minutes and the values range from -32 to 95 dBZ with a 0.5-dBZ-resolution. The DX product features a terrain-based scan-elevation. Due to the flat terrain around the radar site Emden, the scan-elevation is constantly 0.8°.

The total period of investigation lasts from November 2010 to October 2012. The investigation is divided into sub-periods with distinct meteorological conditions. These conditions are: thunderstorm, continuous rain, light snow, strong wind and, high-pressure weather.

Results

In the following, the maps und curves for the wind farm near Delfzijl are given. Subsequently the corresponding figures for the second study area at Eemshaven are shown.

Figure 8 shows the mean reflectivity measured for a 57°-sector southwest to the radar in Emden comprising the wind farm near Delfzijl. Striking is a concentration of higher mean values (up to about 32 dBZ) in a distance of 7 to 9 km from the radar. For the sake of better visual identification of the coordinates, Figure 9 provides a representation of the same data with equal pixel size.

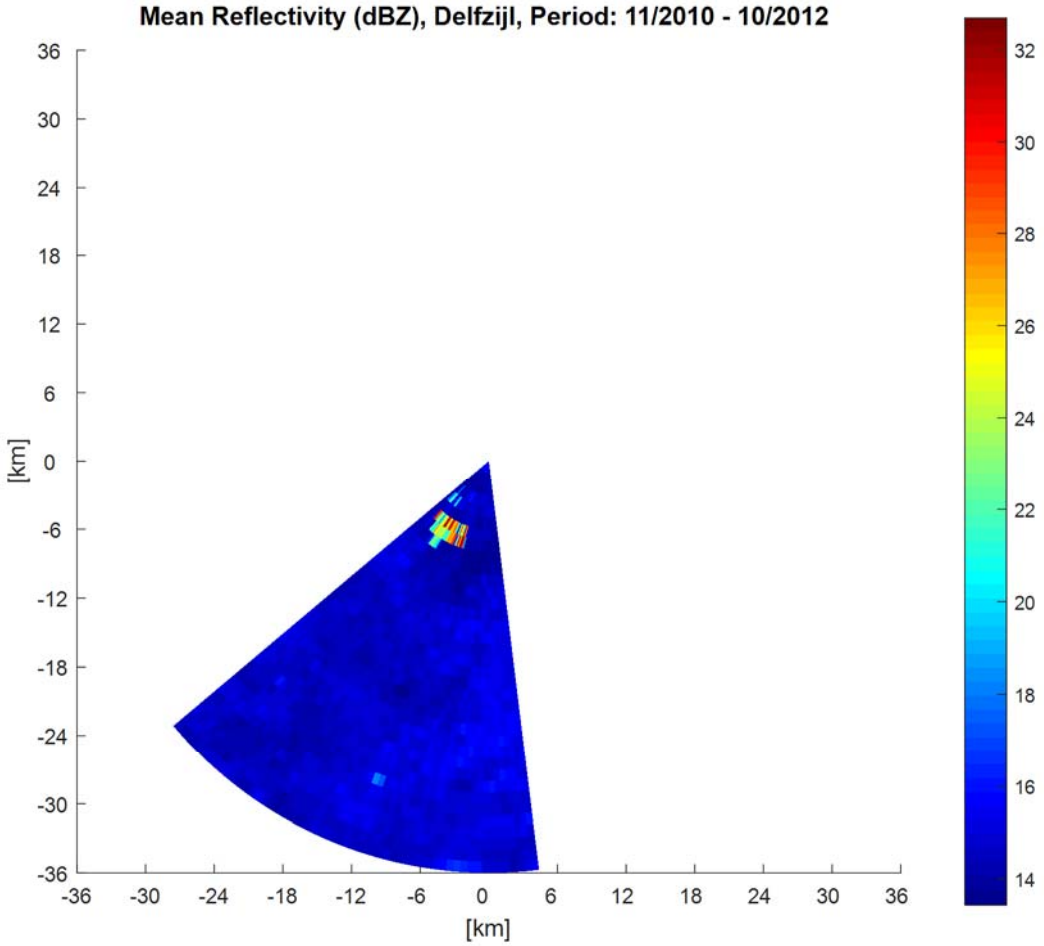


**Figure 8: Mean reflectivity map for a 57°-sector southwest to the radar in Emden.**

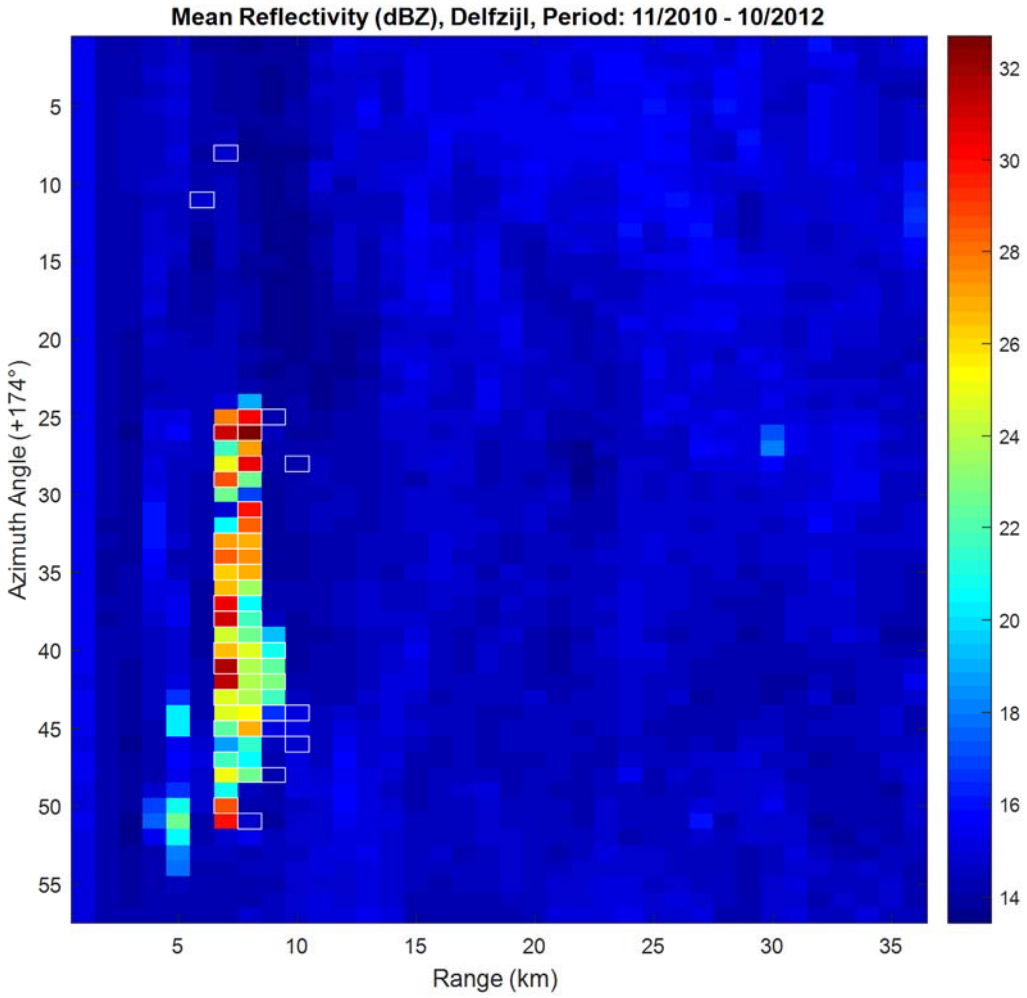


**Figure 9: Mean reflectivity map. The coordinates containing wind turbines in the area of Delfzijl are edged in white.**

It is obvious that not all coordinates comprising one or more wind turbines exhibit strikingly high mean reflectivity values (Annotation: Only wind turbines in the area of Delfzijl are highligted). However, the area of high mean reflectivities coincites with the wind farm.

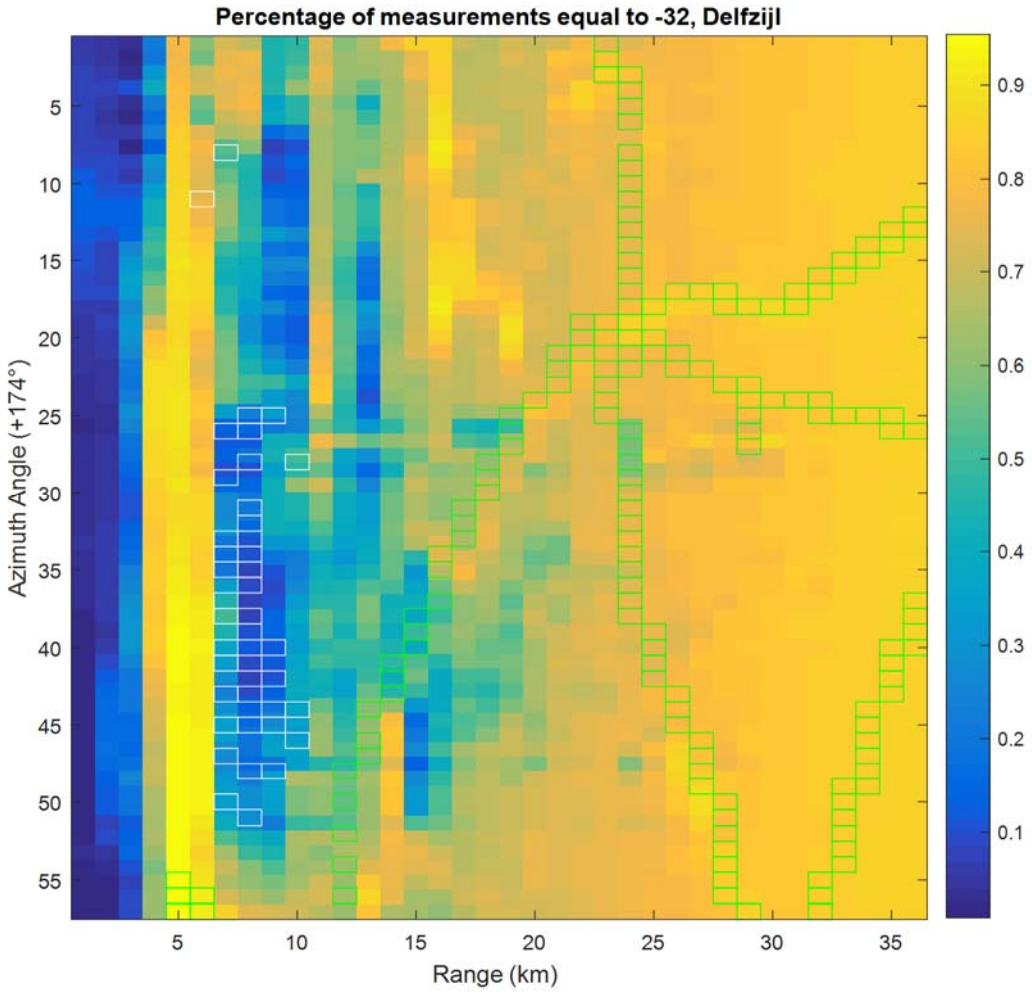


**Figure 10: Map showing the percentage of -32 dBZ-values for each coordinate. The coordinates containing wind turbines in the area of Delfzijl are edged in white. The coordinates containing high-voltage transmission poles are edged in green.**

The area of low percentage of -32 dBZ-values near the radar is the bay area. Low values were also detected at the wind farm. However, some lines with slightly higher values than in their vicinity can be observed along some high-voltage transmission poles. (Annotation: Their position was extracted via OpenStreetMap).

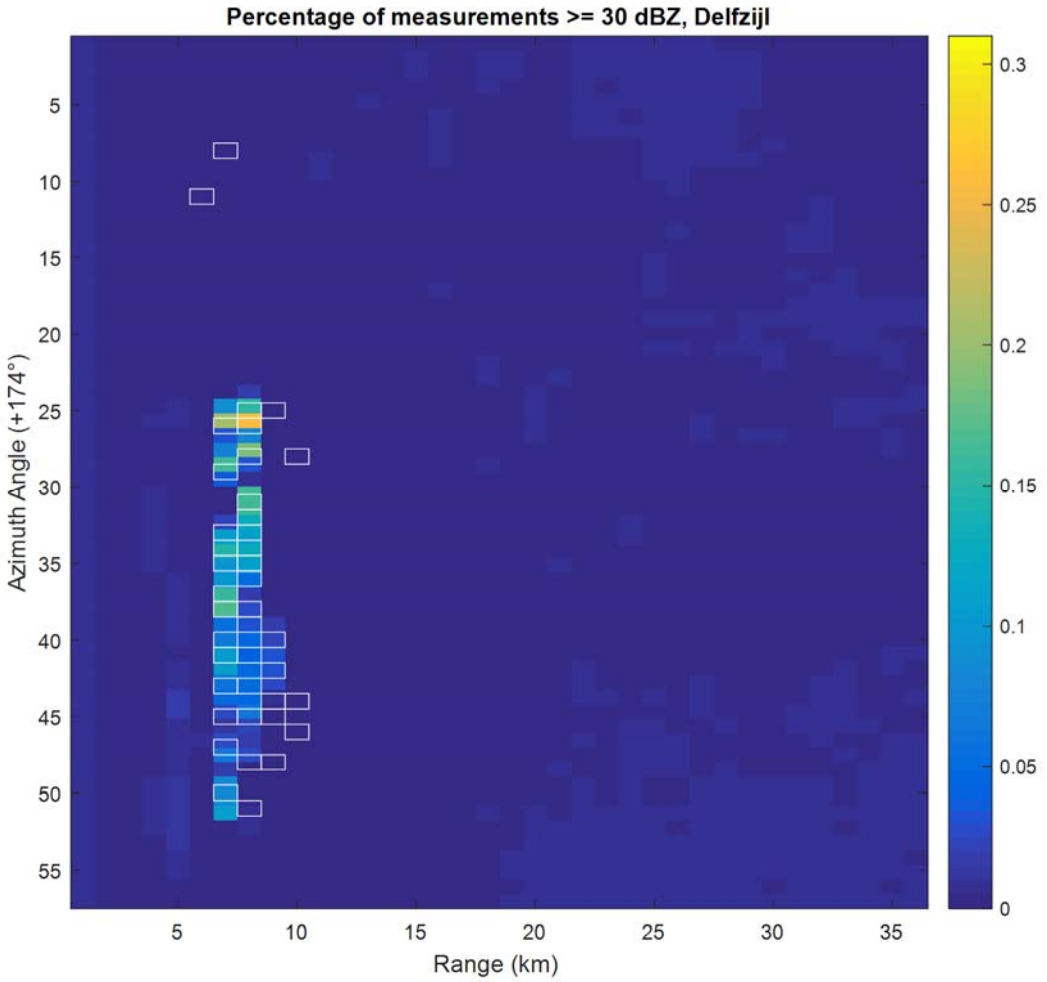


**Figure 11: Map showing the percentage of values >= 30 dBZ for each coordinate. The coordinates containing wind turbines in the area of Delfzijl are edged in white.**

Reflectivities equal to or greater than 30 dBZ are far more frequent at the wind farm coordinates. A value of 0.25 means that over the whole period of two years, one out of four measurements at that coordinate is >=30 dBZ.

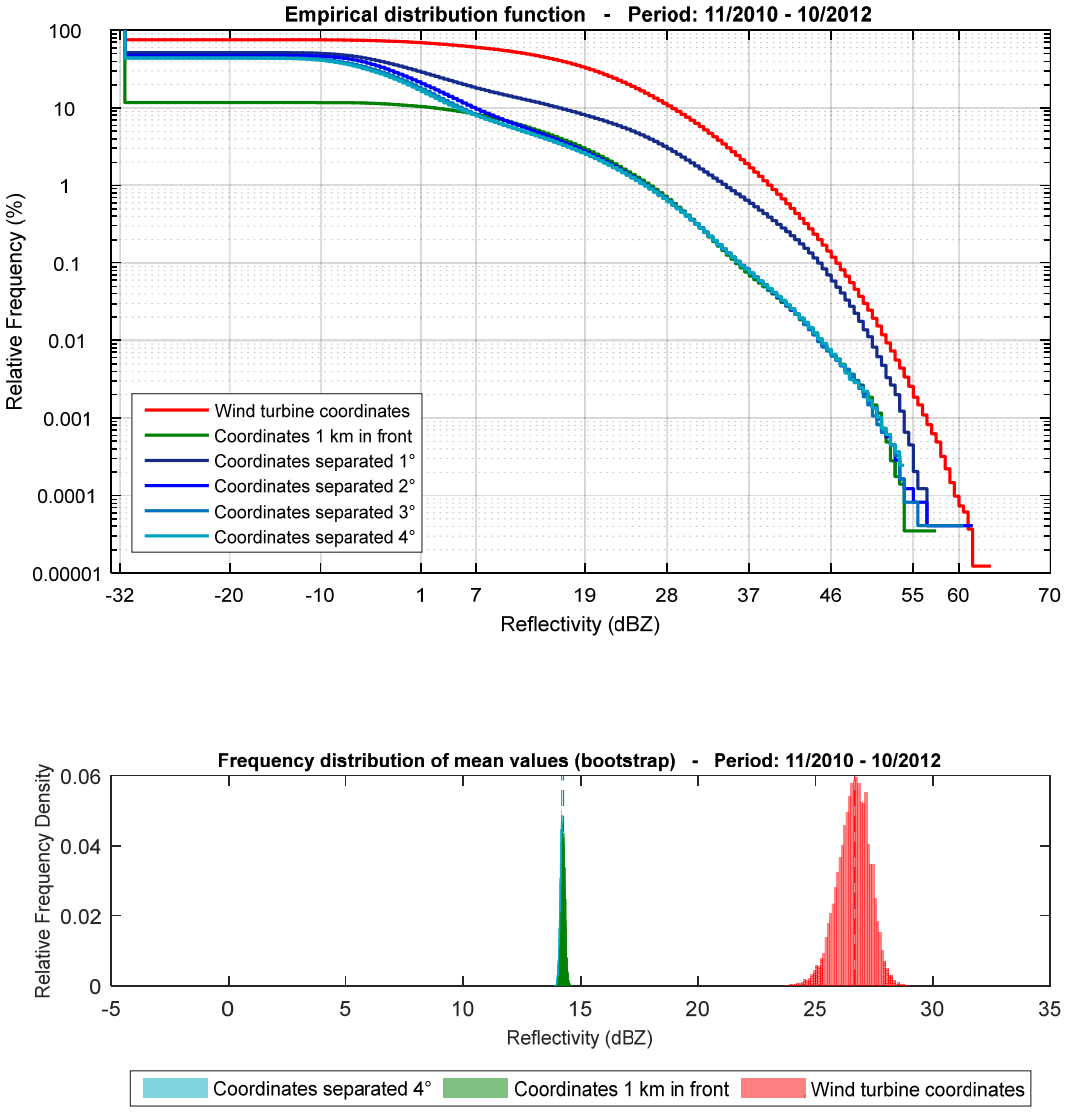


**Figure 12: Empirical CDF for measurements at defined coordinates and bootstrap analysis of the mean values (below).**

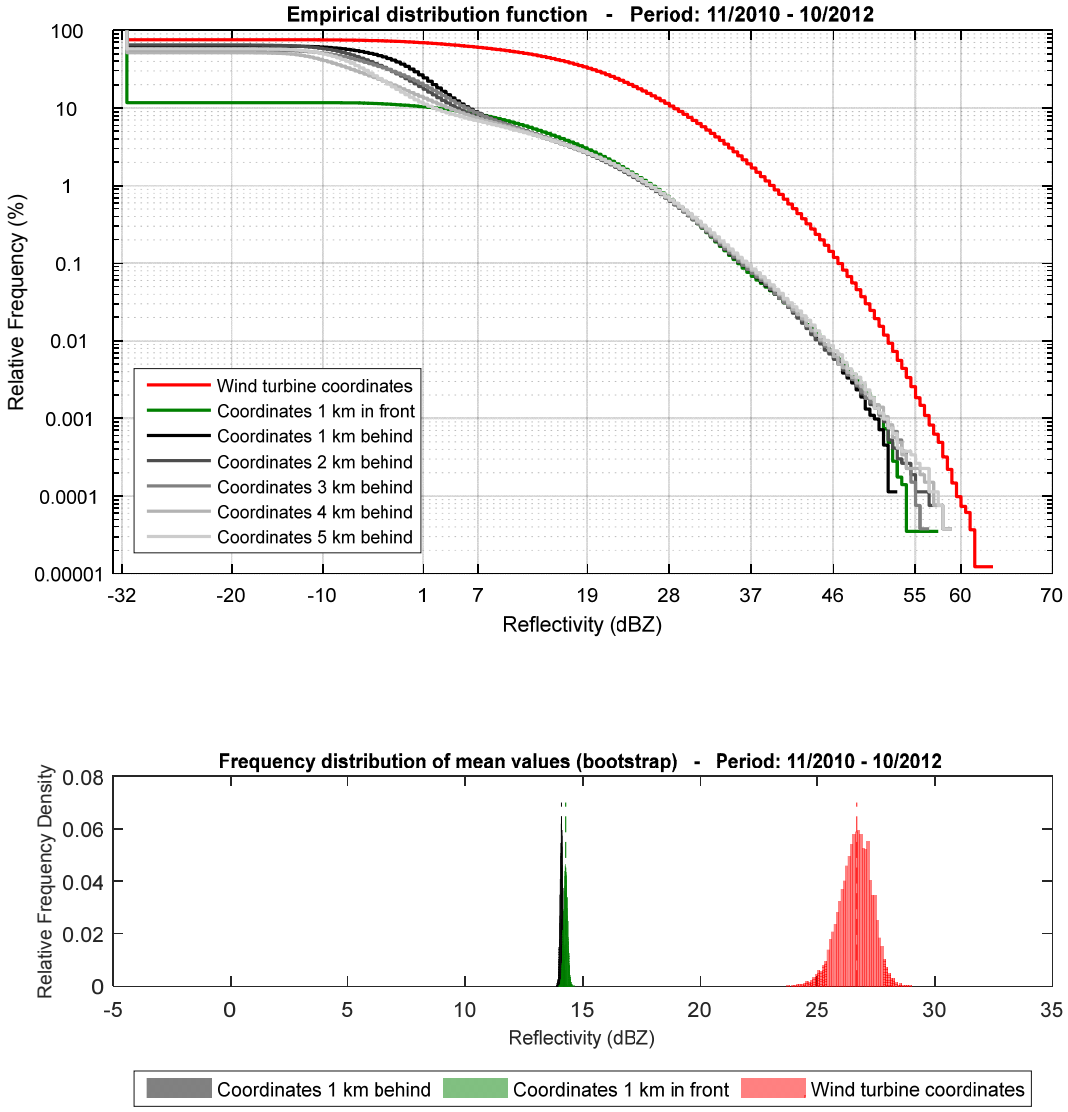


**Figure 13: Empirical CDF for measurements at defined coordinates and bootstrap analysis of the mean values (below).**

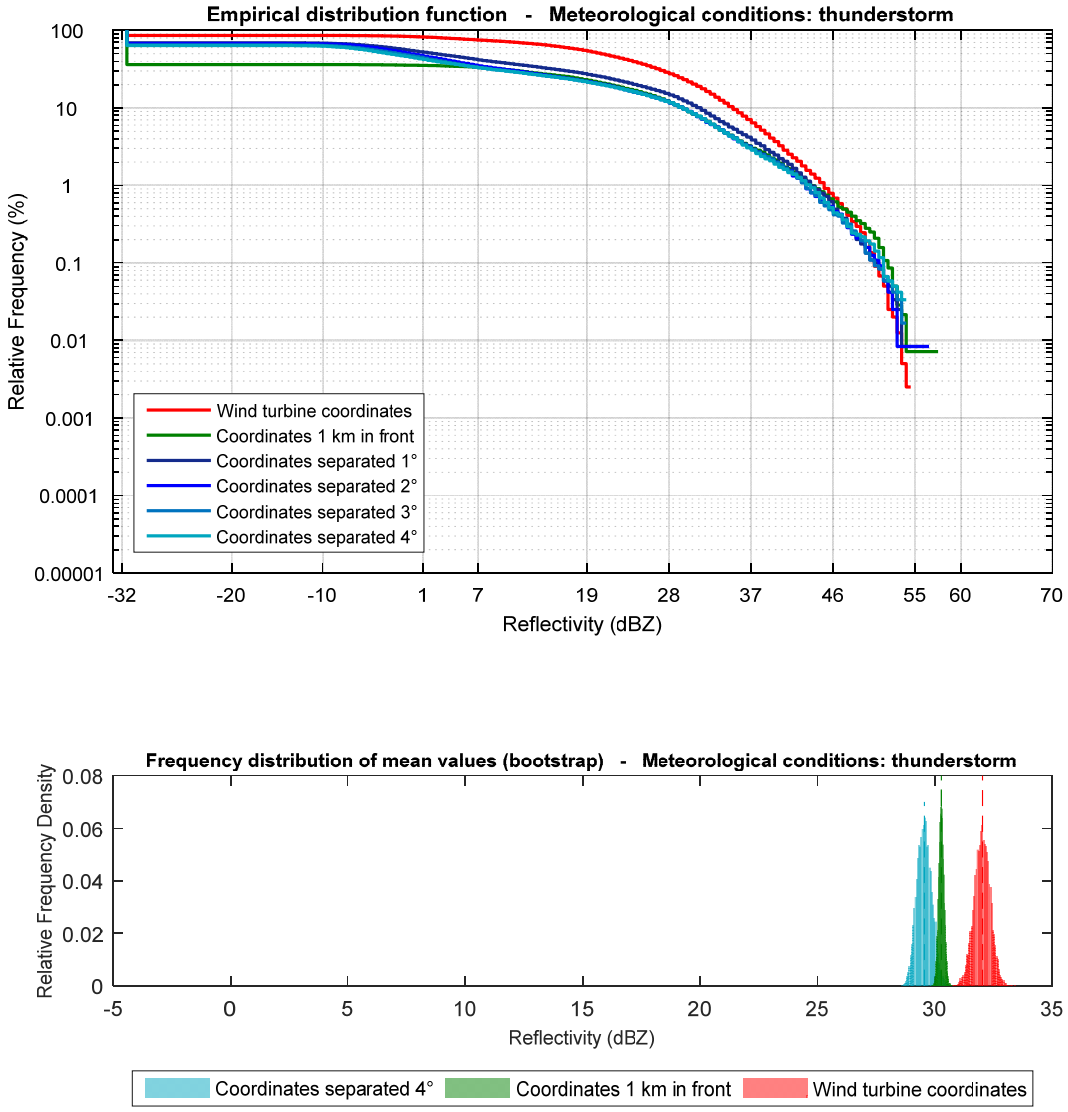


**Figure 14: Empirical CDF for measurements at defined coordinates and meteorological conditions; and bootstrap analysis of the mean values (below).**

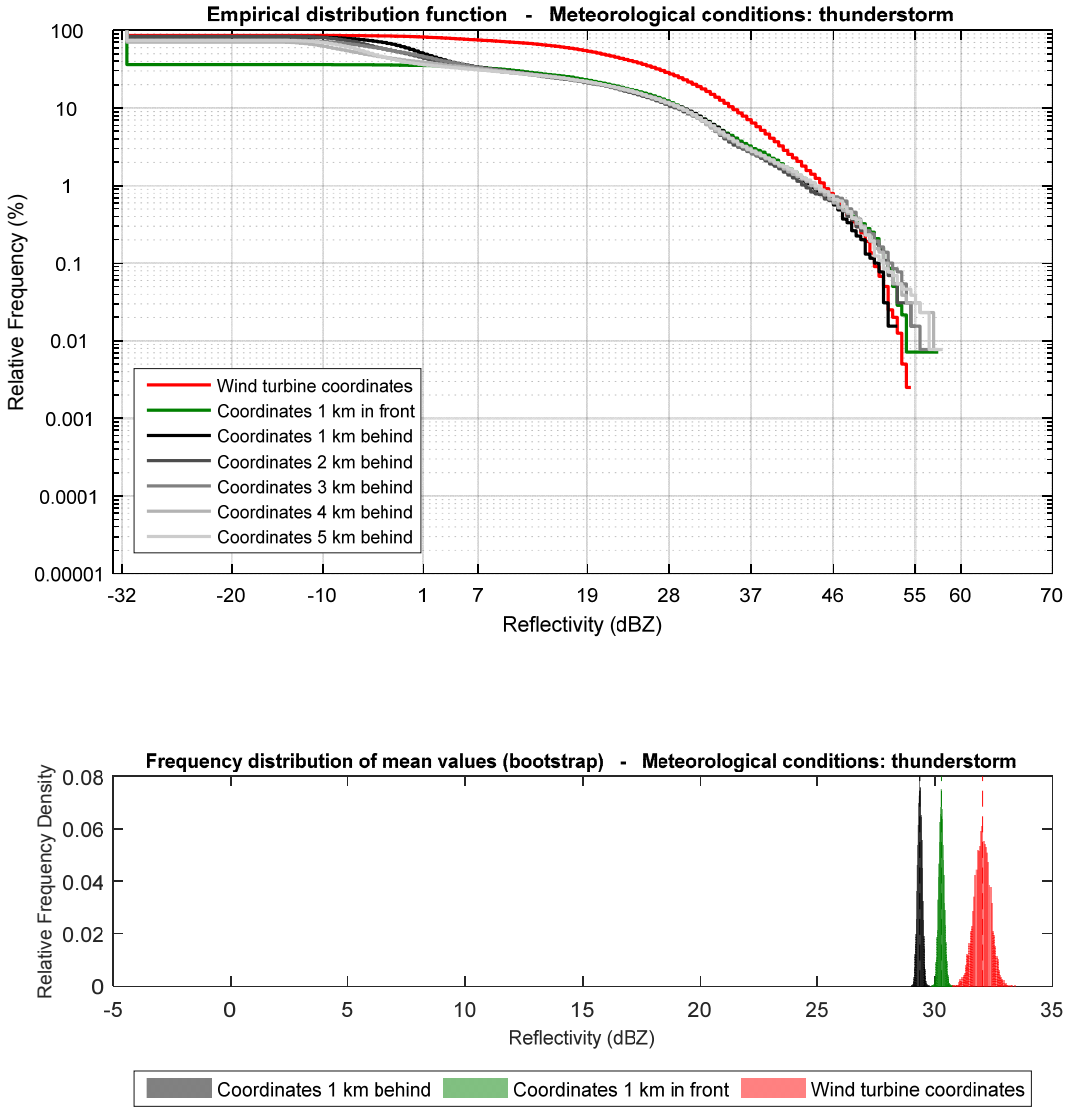


**Figure 15: Empirical CDF for measurements at defined coordinates and meteorological conditions; and bootstrap analysis of the mean values (below).**

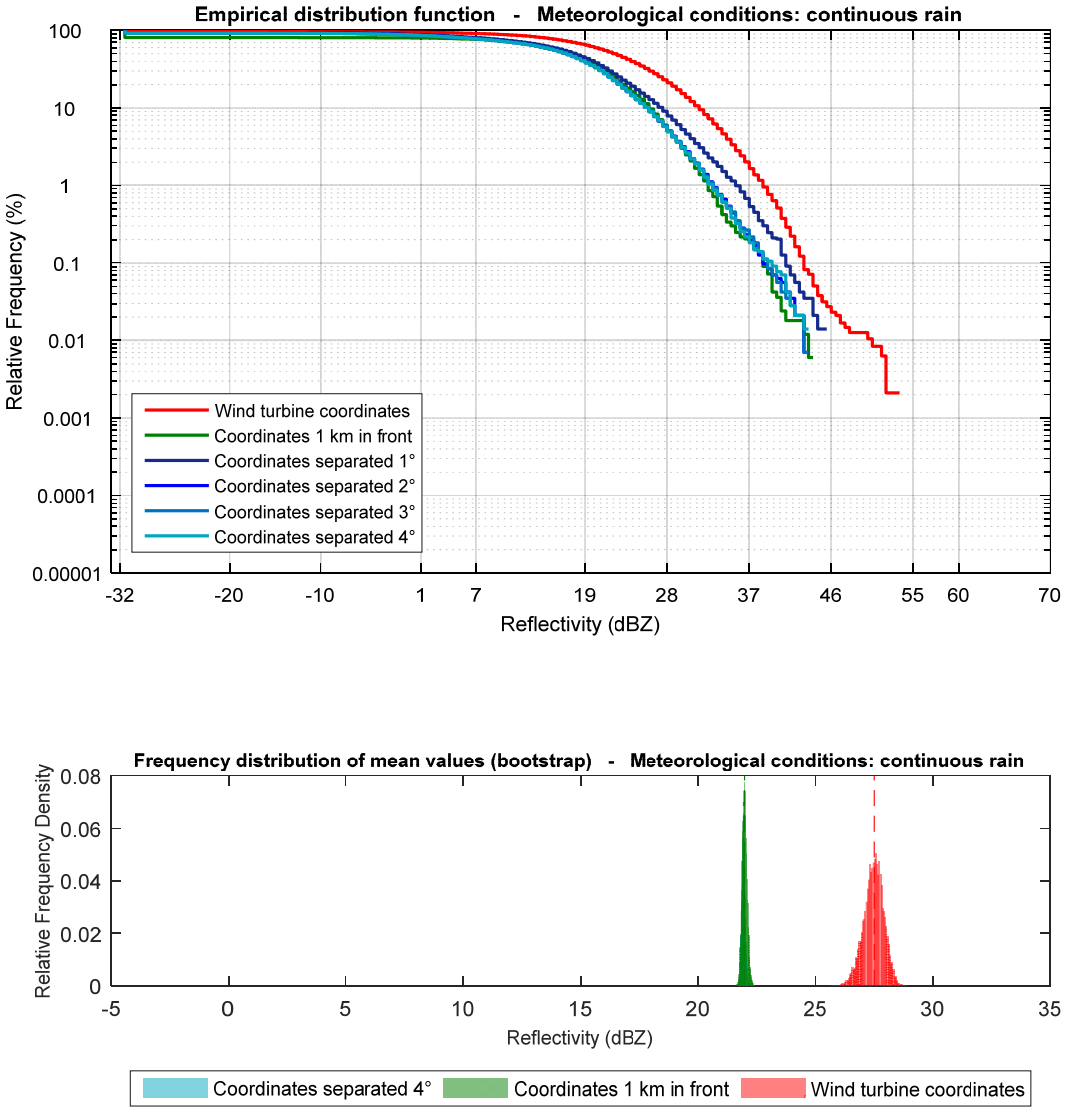


**Figure 16: Empirical CDF for measurements at defined coordinates and meteorological conditions; and bootstrap analysis of the mean values (below).**

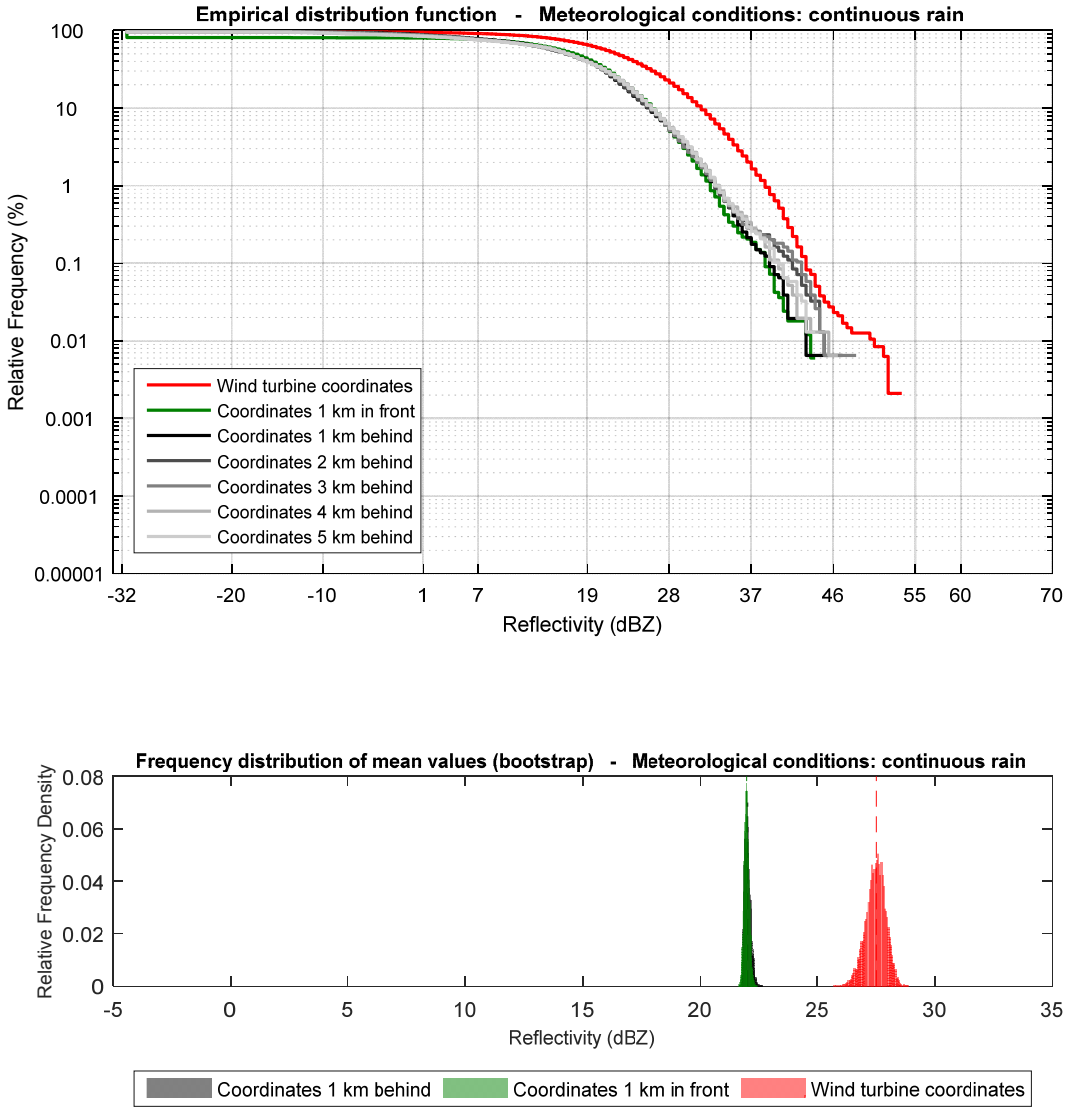


**Figure 17: Empirical CDF for measurements at defined coordinates and meteorological conditions; and bootstrap analysis of the mean values (below).**

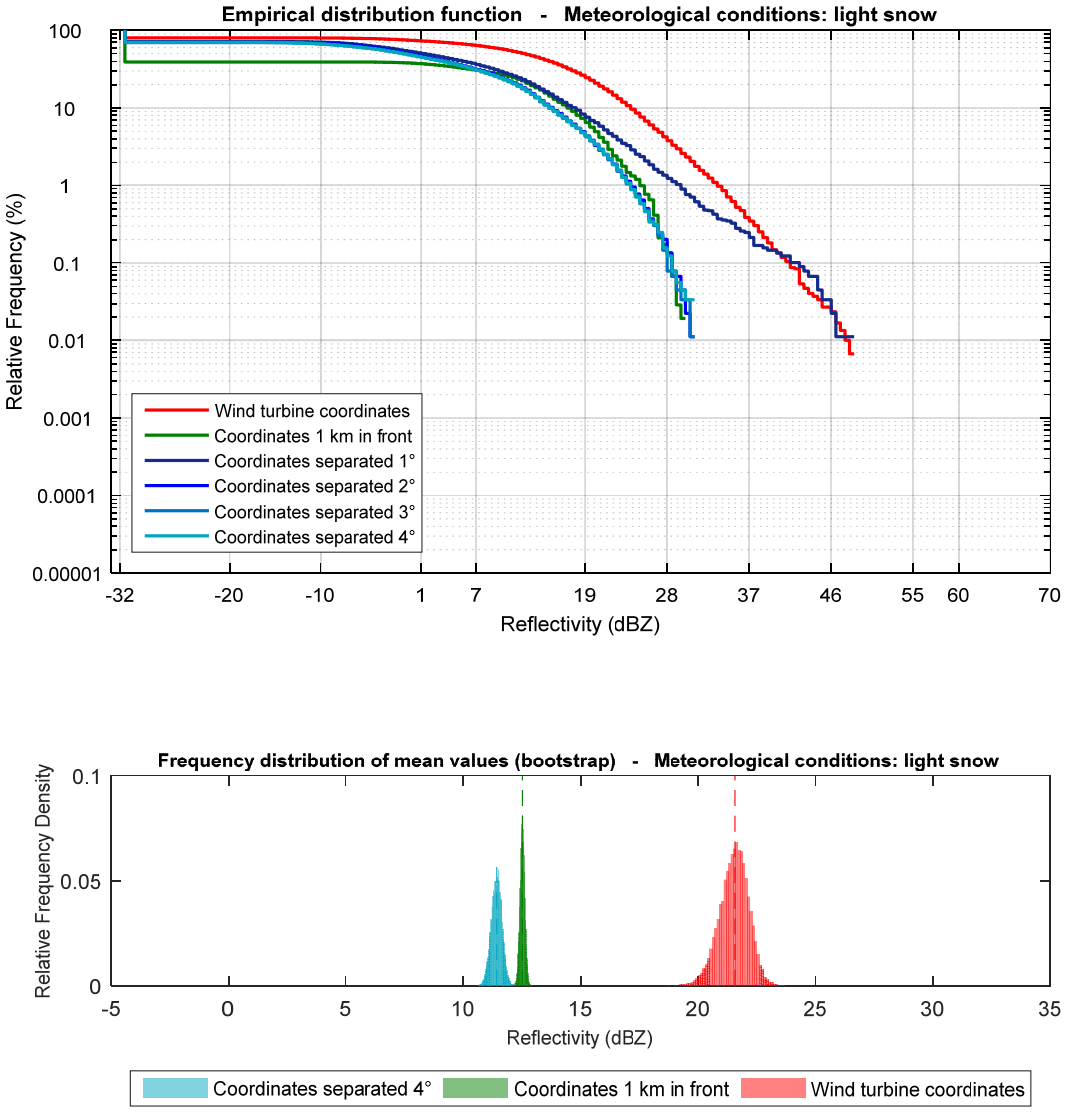


**Figure 18: Empirical CDF for measurements at defined coordinates and meteorological conditions; and bootstrap analysis of the mean values (below).**

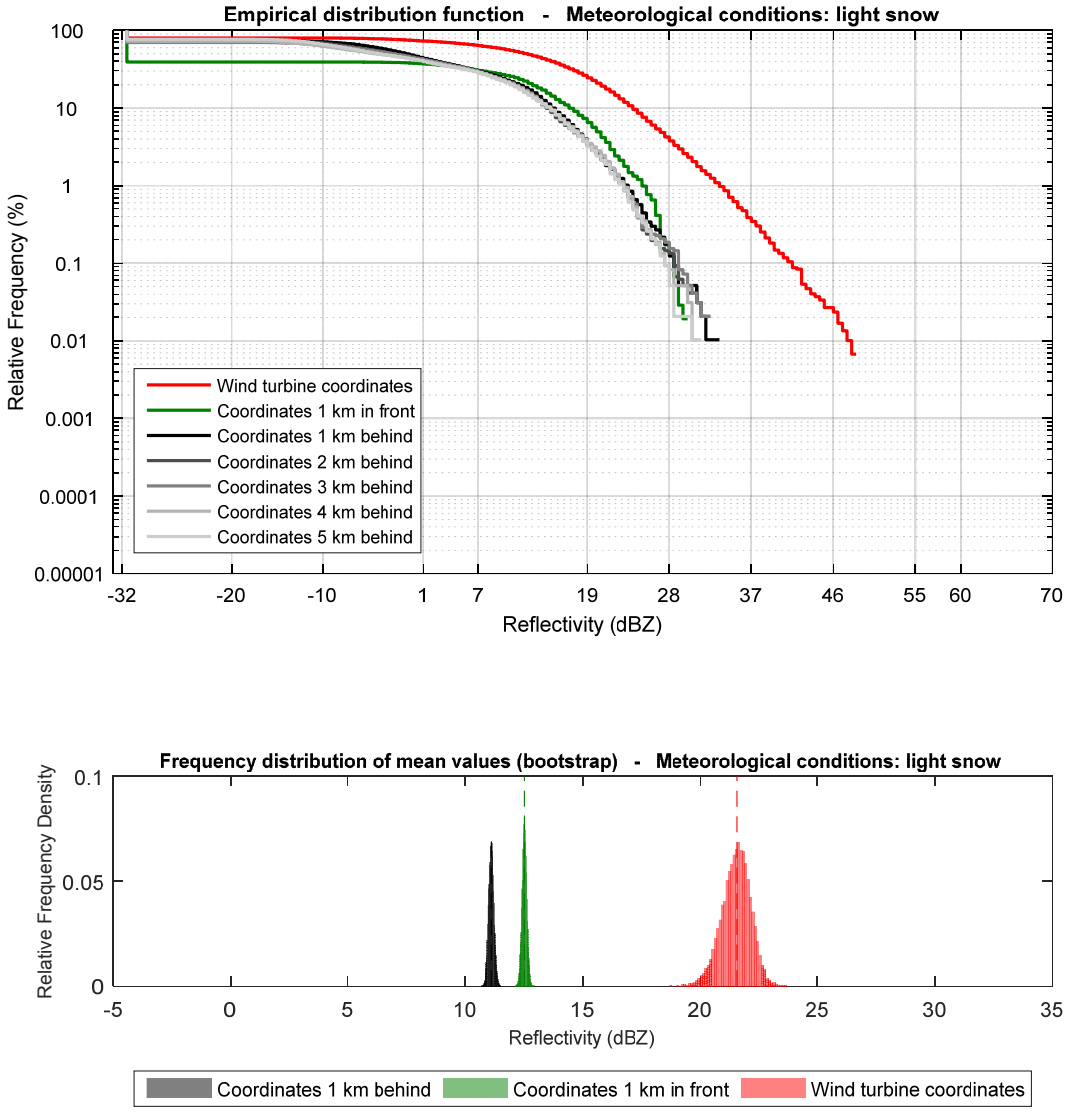


**Figure 19: Empirical CDF for measurements at defined coordinates and meteorological conditions; and bootstrap analysis of the mean values (below).**

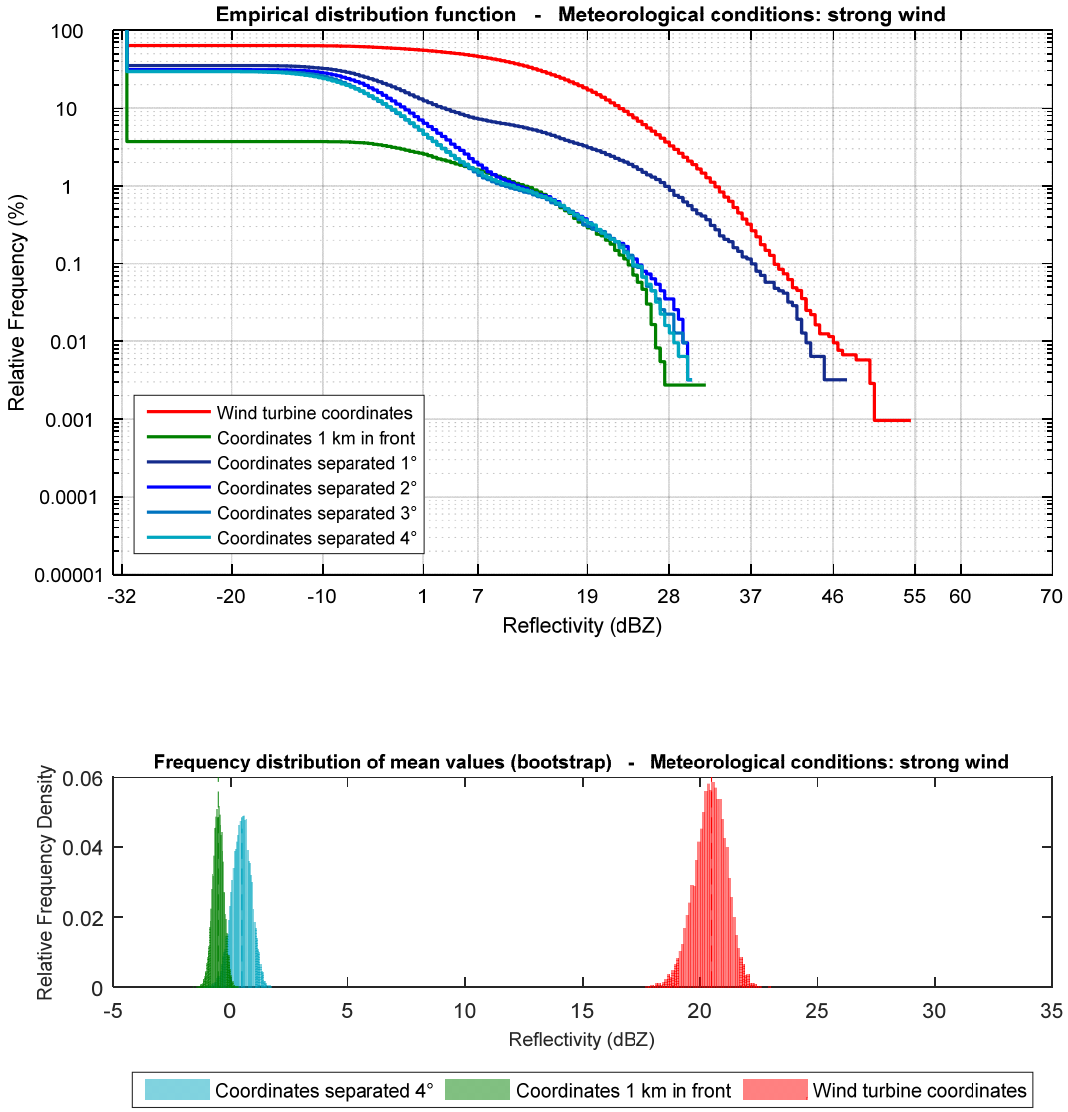


**Figure 20: Empirical CDF for measurements at defined coordinates and meteorological conditions; and bootstrap analysis of the mean values (below).**

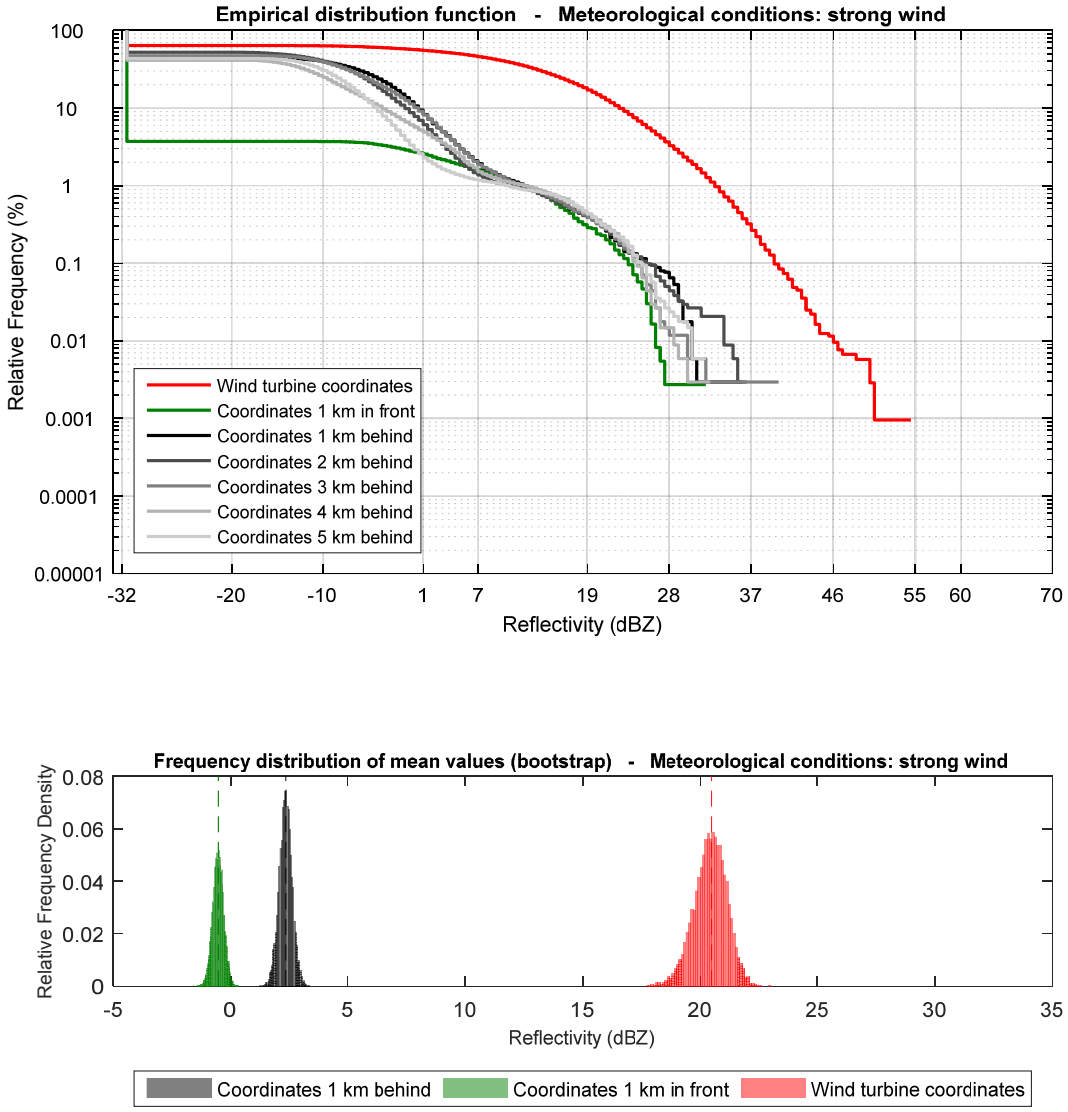


**Figure 21: Empirical CDF for measurements at defined coordinates and meteorological conditions; and bootstrap analysis of the mean values (below).**

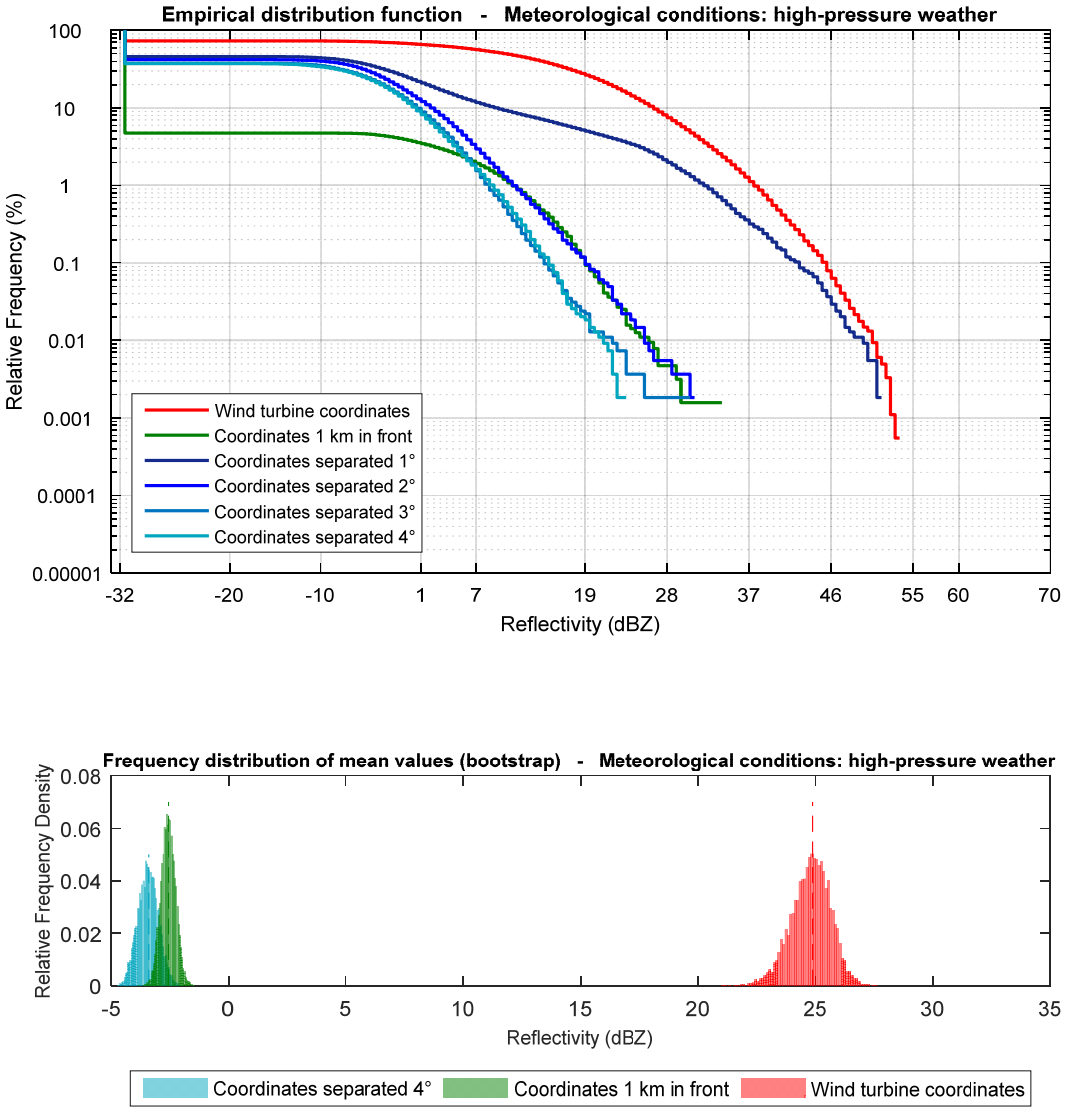


**Figure 22: Empirical CDF for measurements at defined coordinates and meteorological conditions; and bootstrap analysis of the mean values (below).**

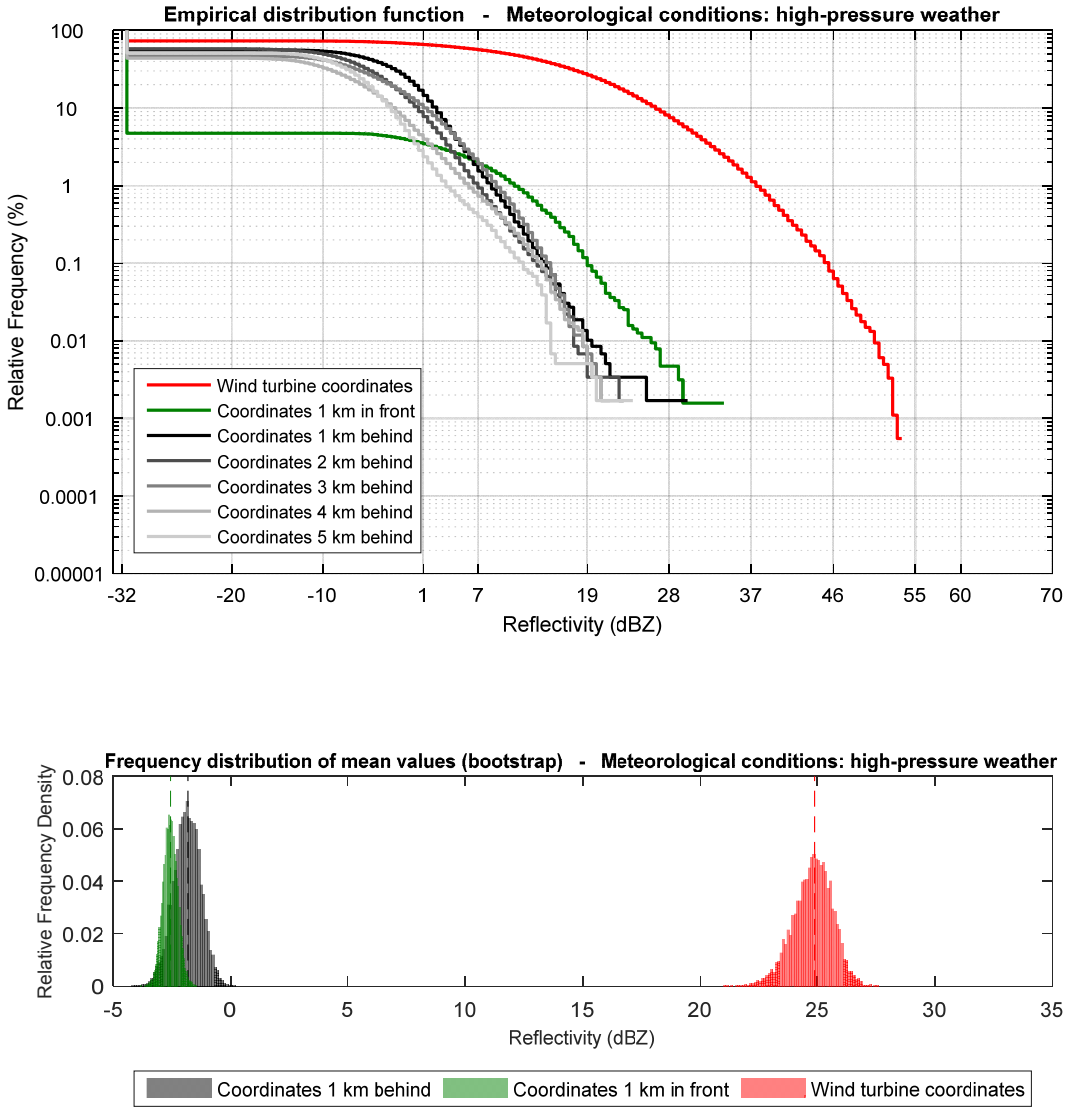


**Figure 23: Empirical CDF for measurements at defined coordinates and meteorological conditions; and bootstrap analysis of the mean values (below).**

In the following, the maps und curves for the wind farm near Eemshaven are shown. Analogous to the situation in Delfzijl the area of high mean reflectivities coincites with the wind farm (Figure 25). Noteworthy are some coordinates without wind turbines within the wind farm (due to the contrast best visible in Figure 27). At this location a lower percentage of reflectivities equal to or greater than 30 dBZ and a high percentage of -32 dBZ-values can be observed (with respect to the vicinity, Figure 26)

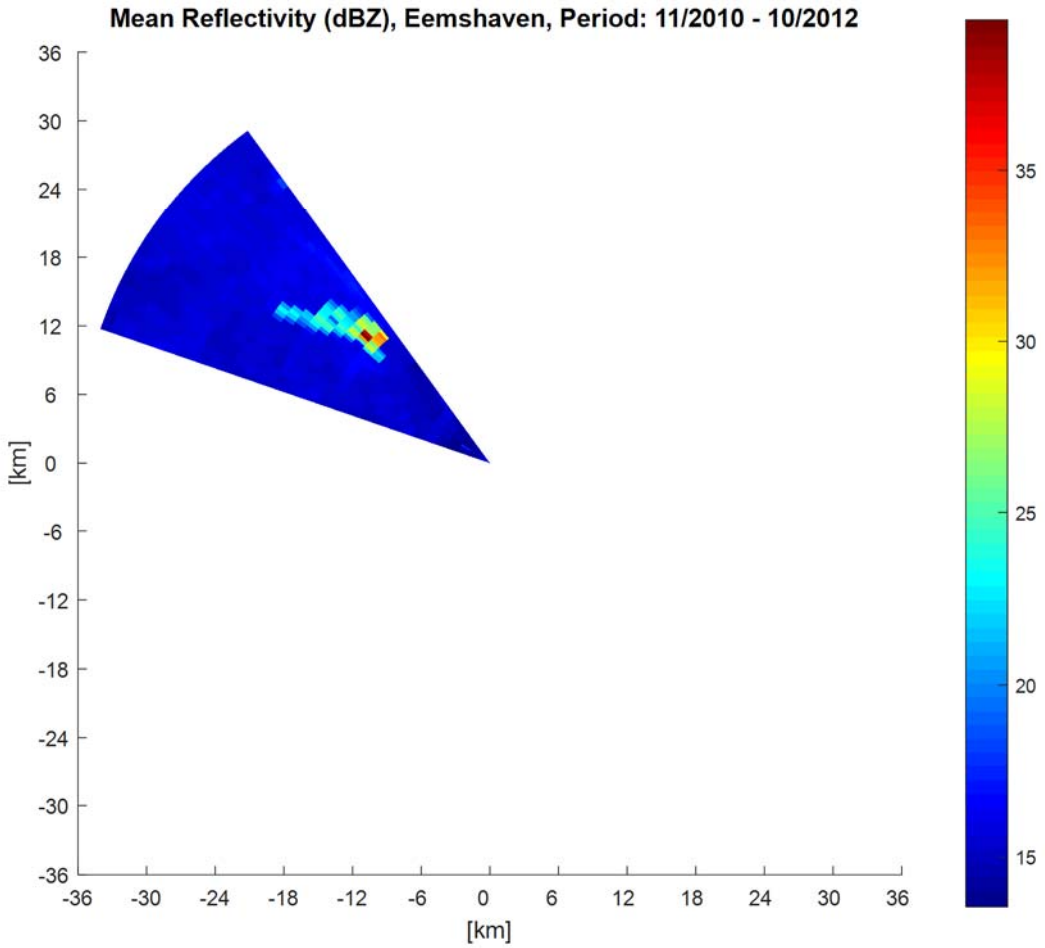


**Figure 24: Mean reflectivity map for a 35°-sector northwest to the radar in Emden.**

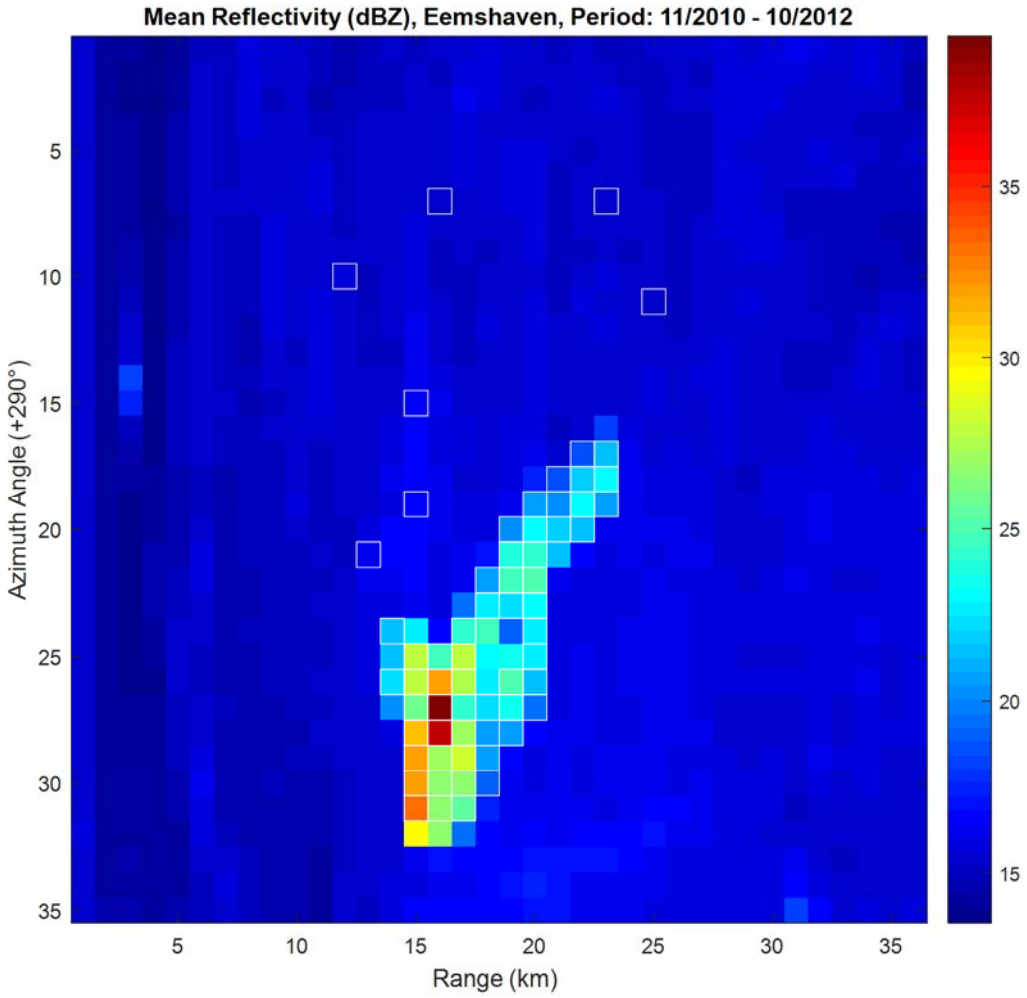


**Figure 25: Mean reflectivity map. The coordinates containing wind turbines in the area of Eemshaven are edged in white.**

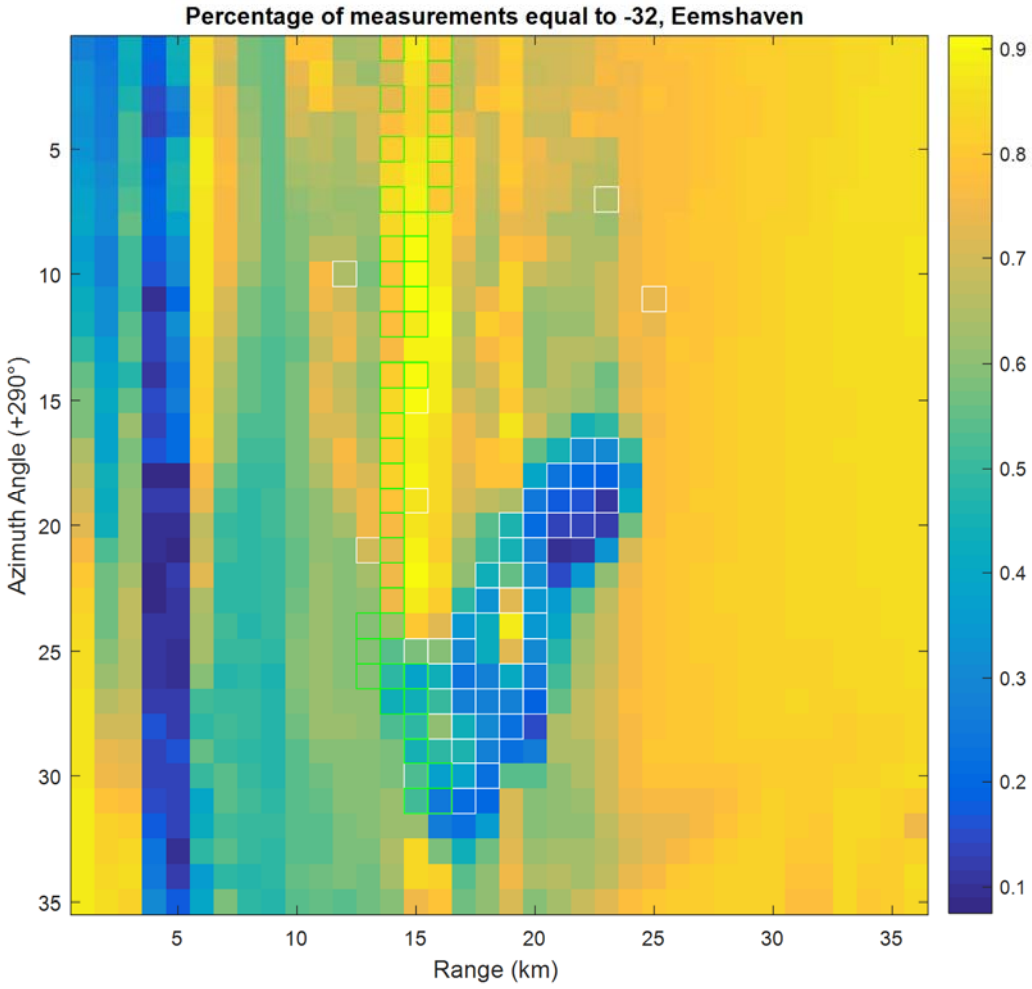


**Figure 26: Map showing the percentage of -32 dBZ-values for each coordinate. The coordinates containing wind turbines in the area of Eemshaven are edged in white. The coordinates containing high-voltage transmission poles are edged in green.**

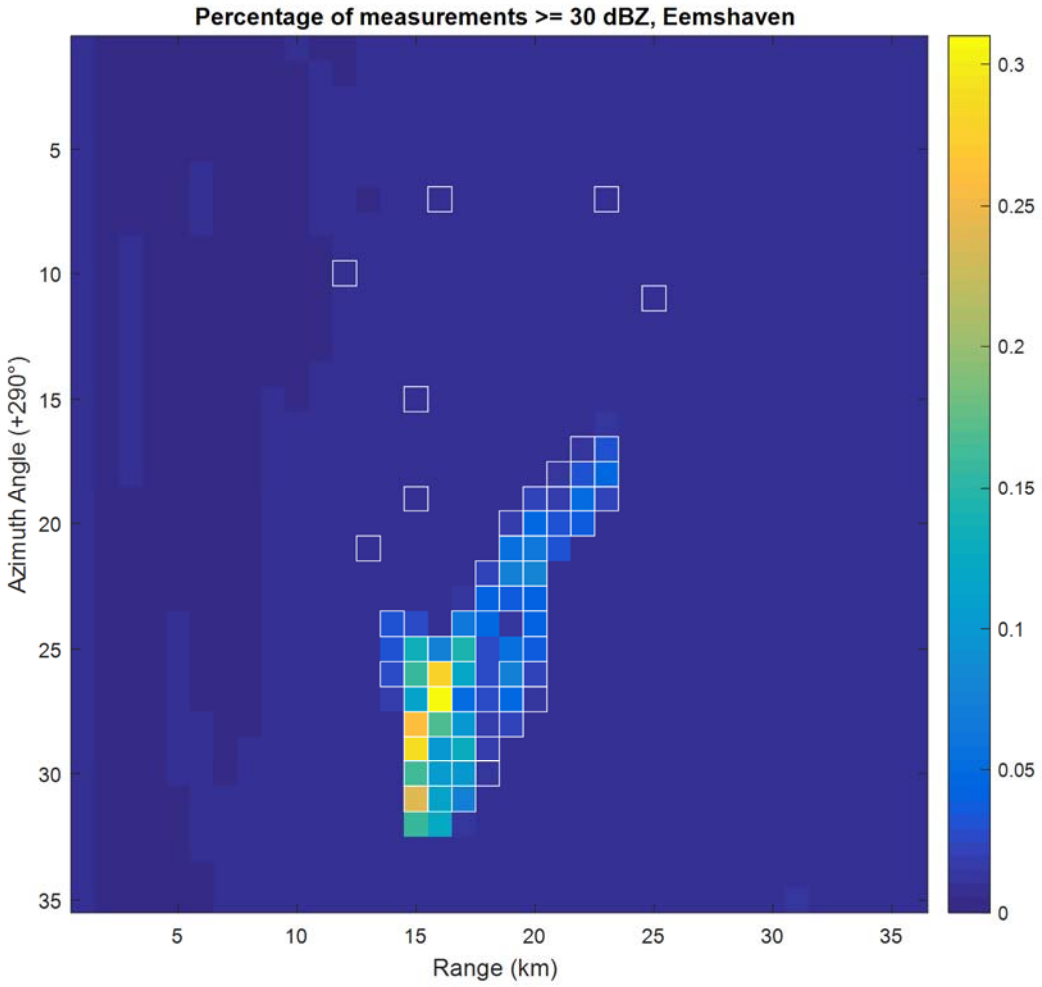


**Figure 27: Map showing the percentage of values >= 30 dBZ for each coordinate. The coordinates containing wind turbines in the area of Eemshaven are edged in white.**

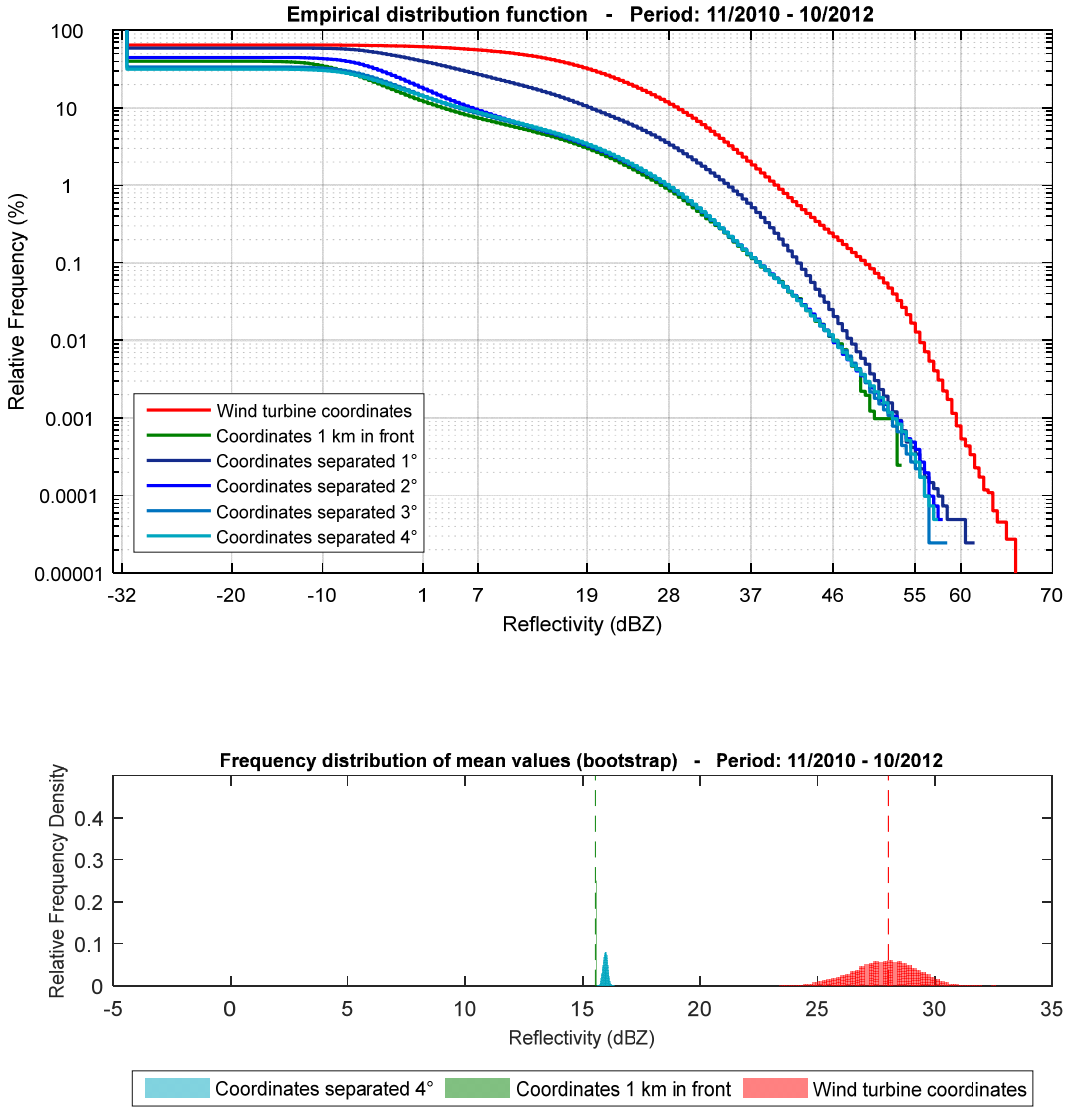


**Figure 28: Empirical CDF for measurements at defined coordinates and bootstrap analysis of the mean values (below).**

In terms of the relative frequency of the occurrence of reflectivity values of a certain magnitude it can be observed that coordinates separated only 1° from wind turbine coordinates show more often higher reflectivities than coordinates with an higher angular distance (Figure 28). This is in accordance with the situation at the wind farm in Delfzijl (Figure 12).

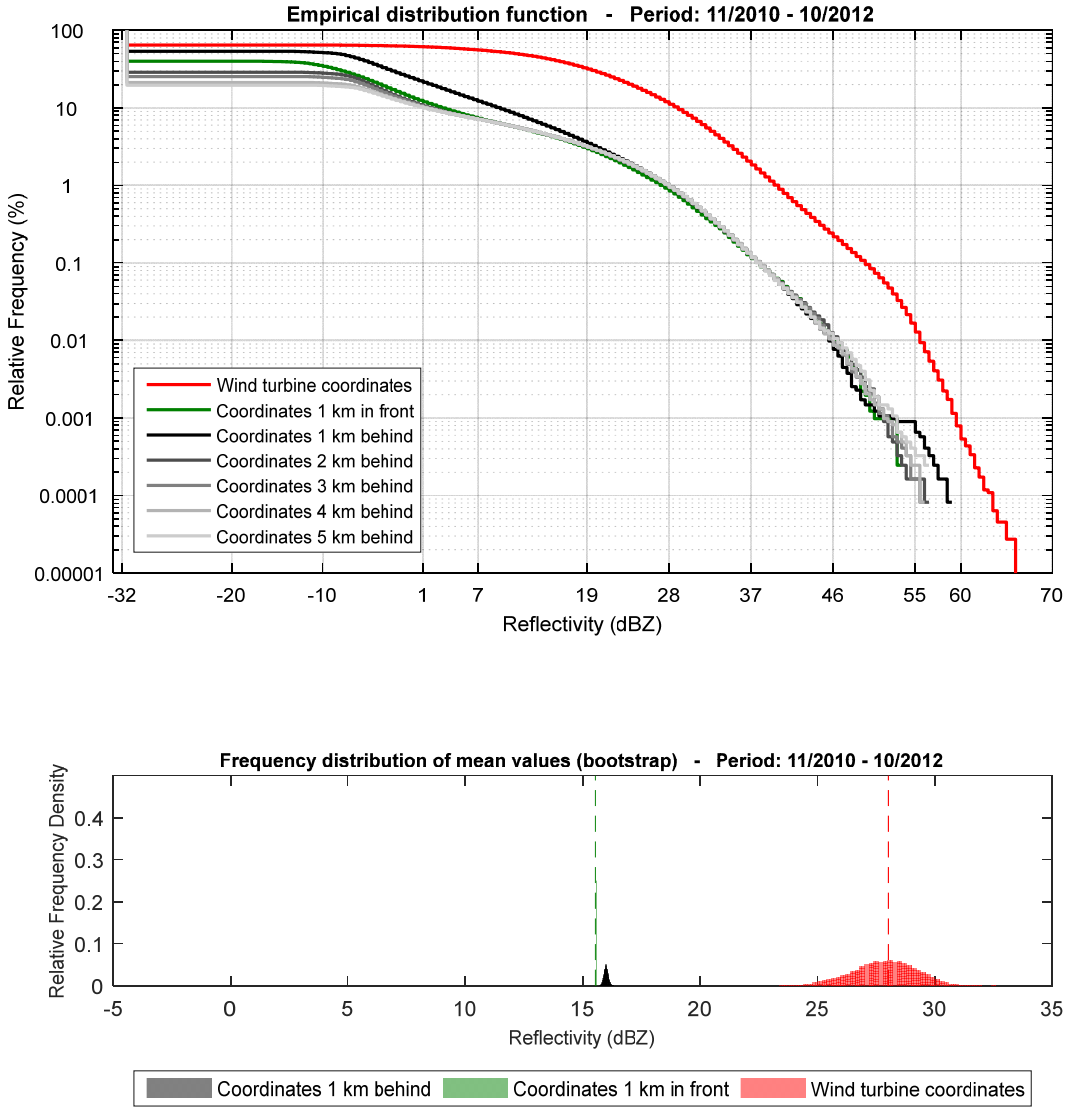


**Figure 29: Empirical CDF for measurements at defined coordinates and bootstrap analysis of the mean values (below).**

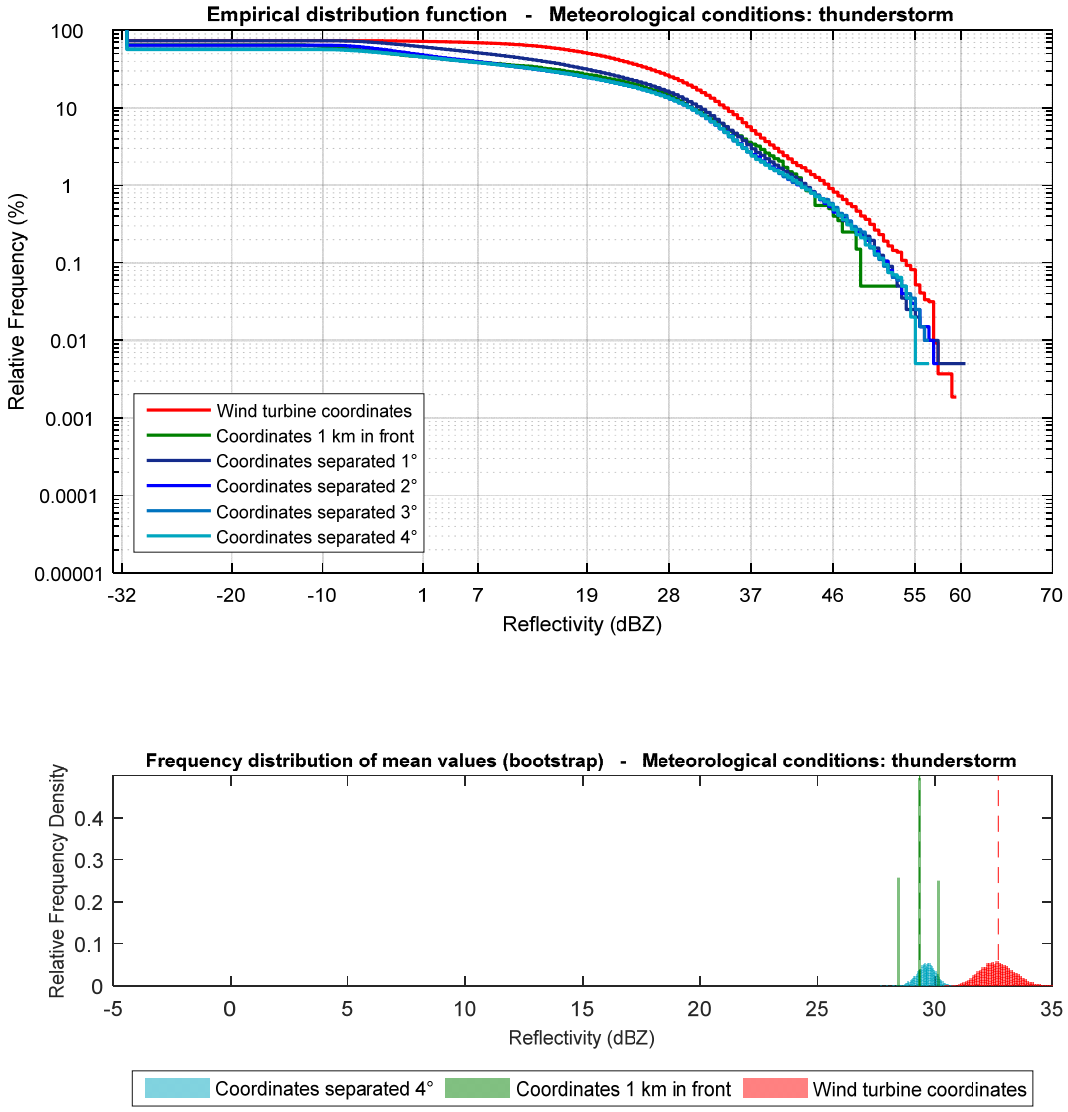


**Figure 30: Empirical CDF for measurements at defined coordinates and meteorological conditions; and bootstrap analysis of the mean values (below).**

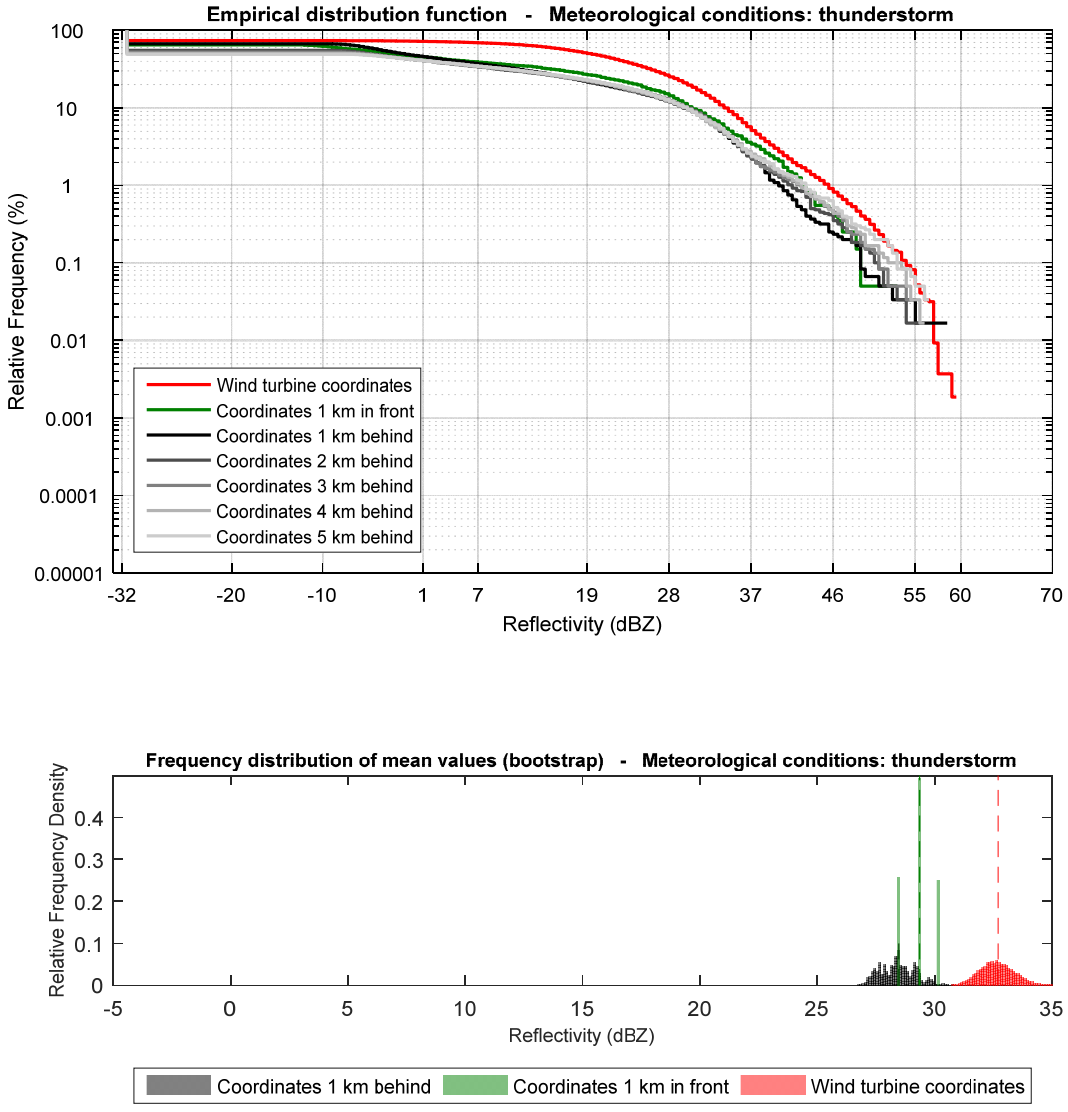


**Figure 31: Empirical CDF for measurements at defined coordinates and meteorological conditions; and bootstrap analysis of the mean values (below).**

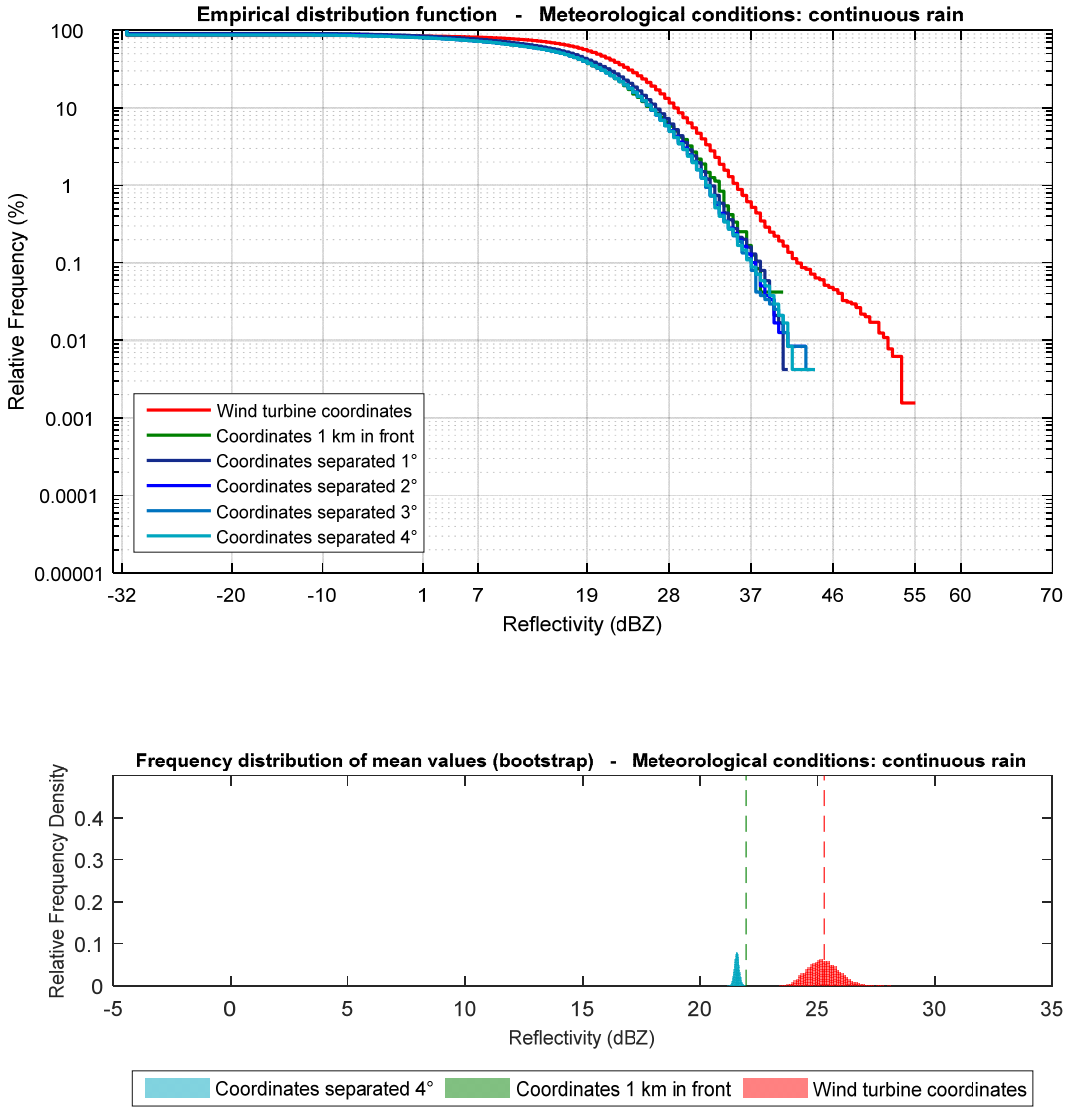


**Figure 32: Empirical CDF for measurements at defined coordinates and meteorological conditions; and bootstrap analysis of the mean values (below).**

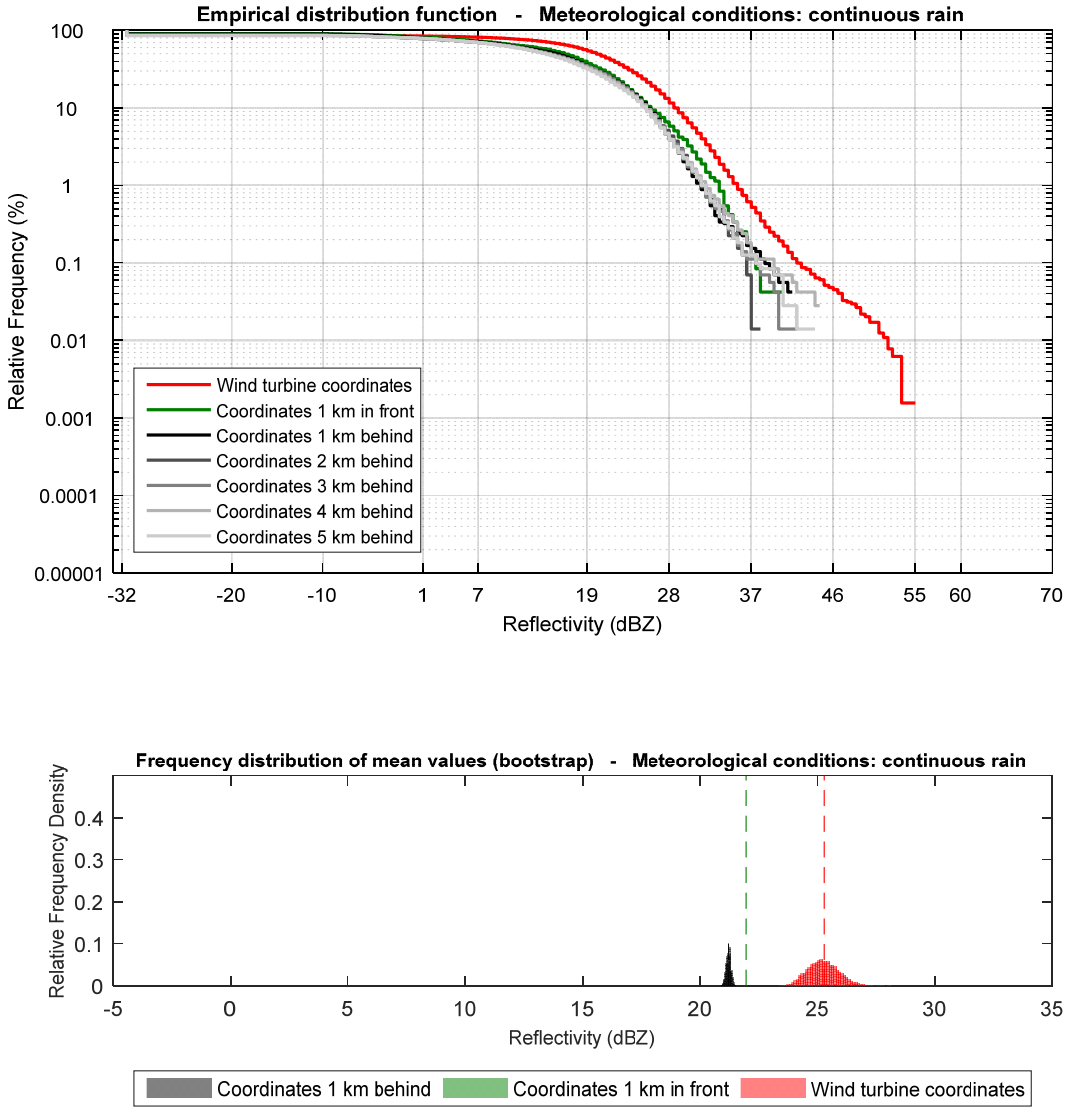


**Figure 33: Empirical CDF for measurements at defined coordinates and meteorological conditions; and bootstrap analysis of the mean values (below).**

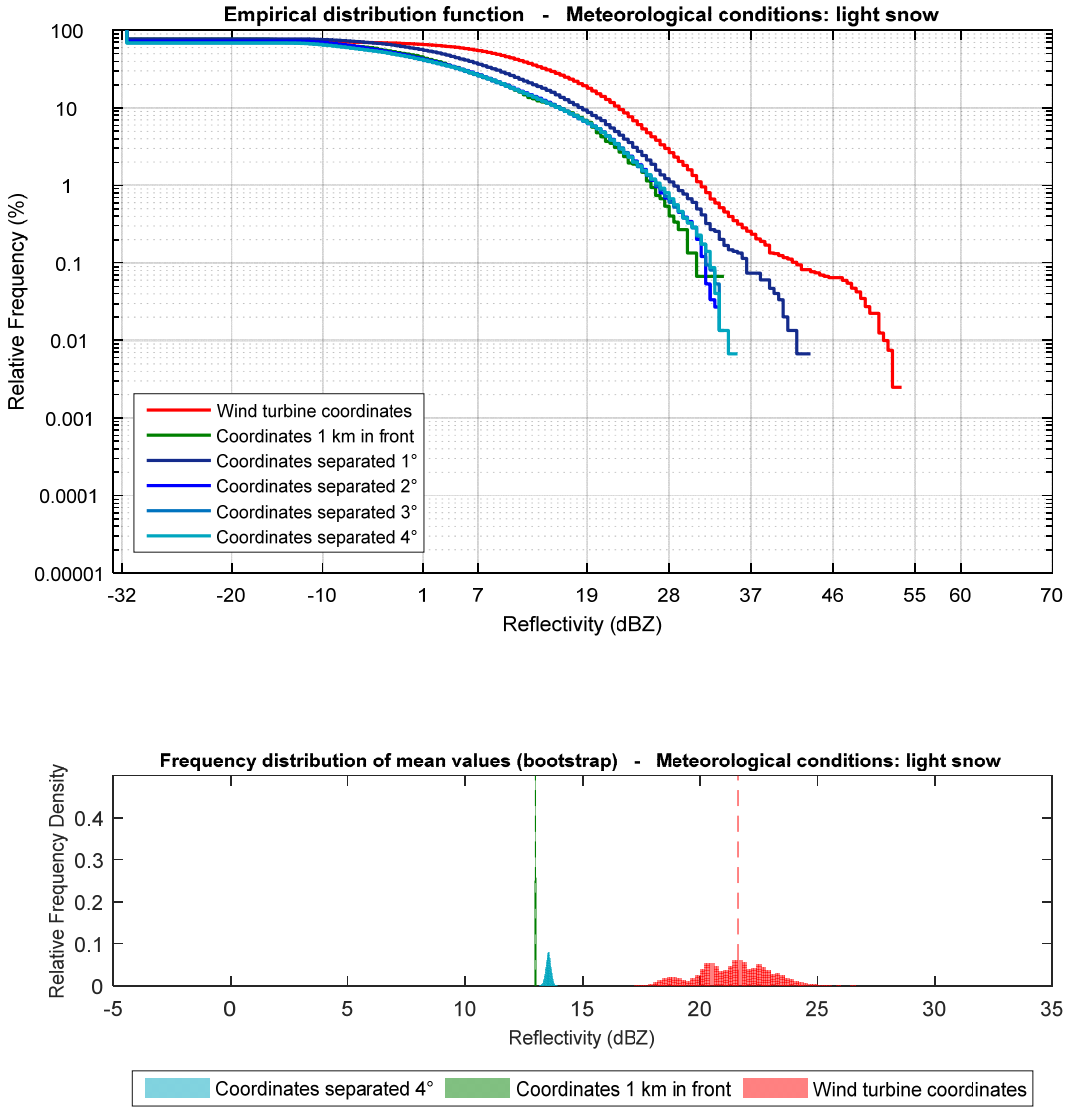


**Figure 34: Empirical CDF for measurements at defined coordinates and meteorological conditions; and bootstrap analysis of the mean values (below).**

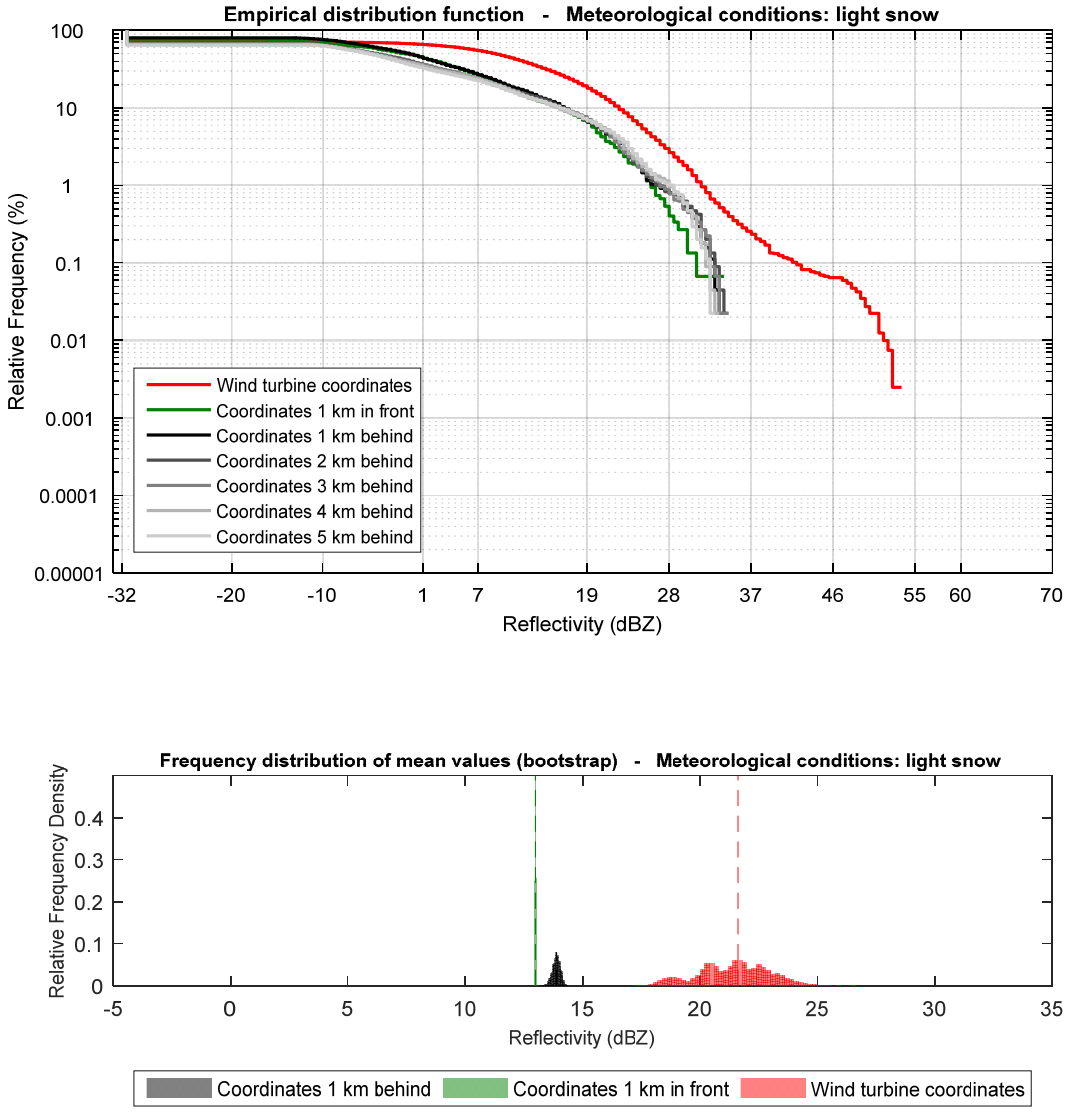


**Figure 35: Empirical CDF for measurements at defined coordinates and meteorological conditions; and bootstrap analysis of the mean values (below).**

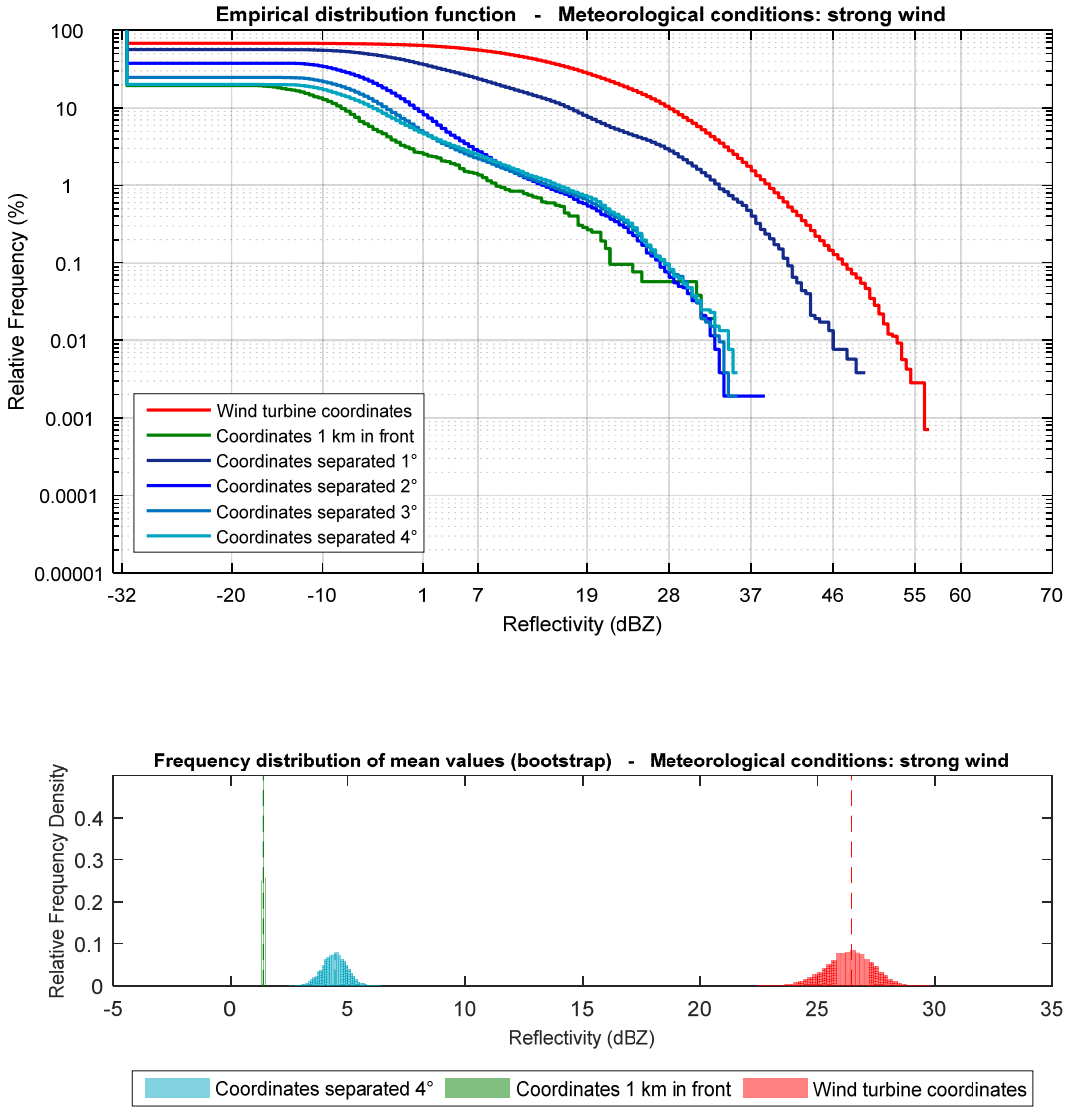


**Figure 36: Empirical CDF for measurements at defined coordinates and meteorological conditions; and bootstrap analysis of the mean values (below).**

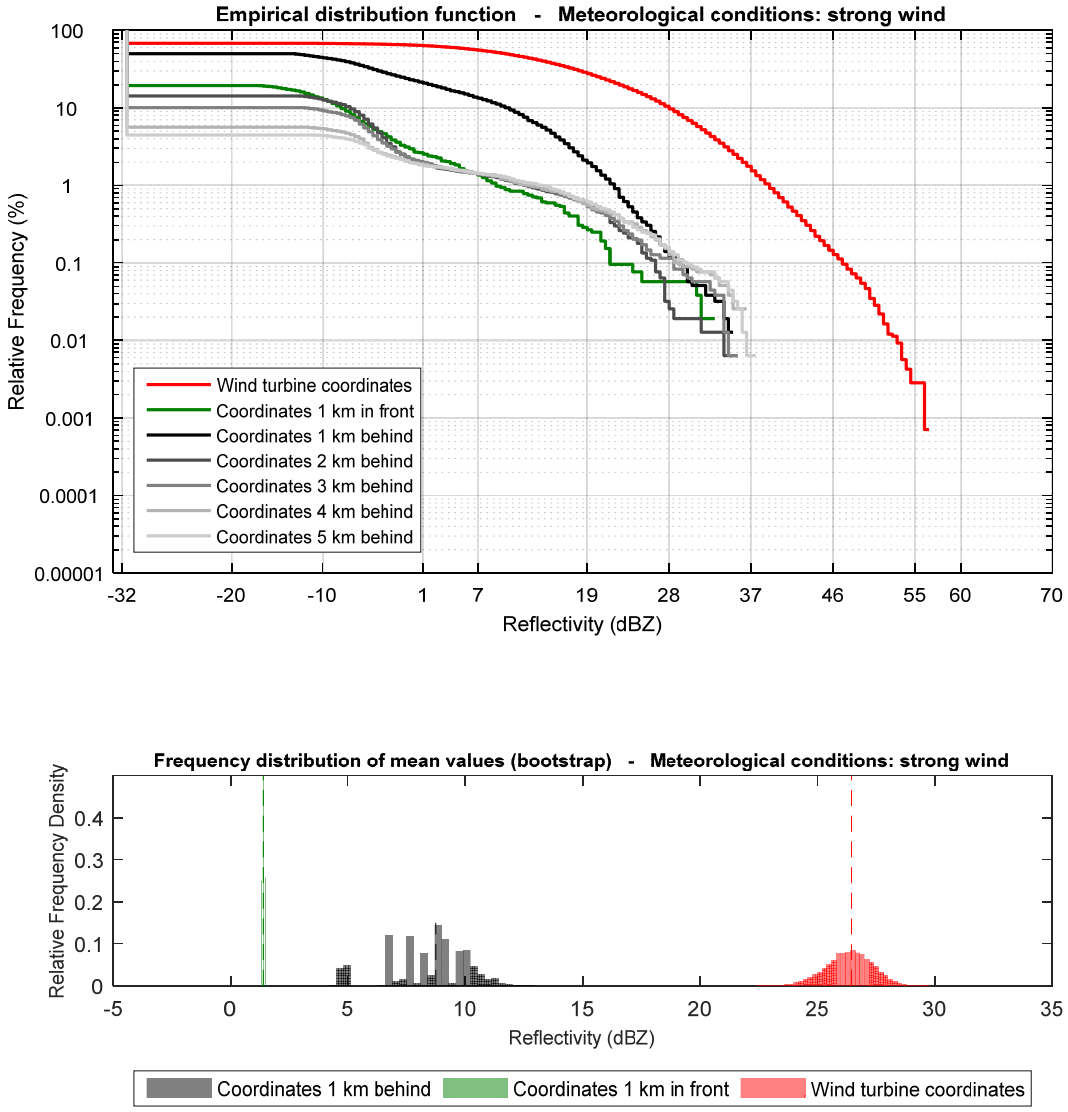


**Figure 37: Empirical CDF for measurements at defined coordinates and meteorological conditions; and bootstrap analysis of the mean values (below).**

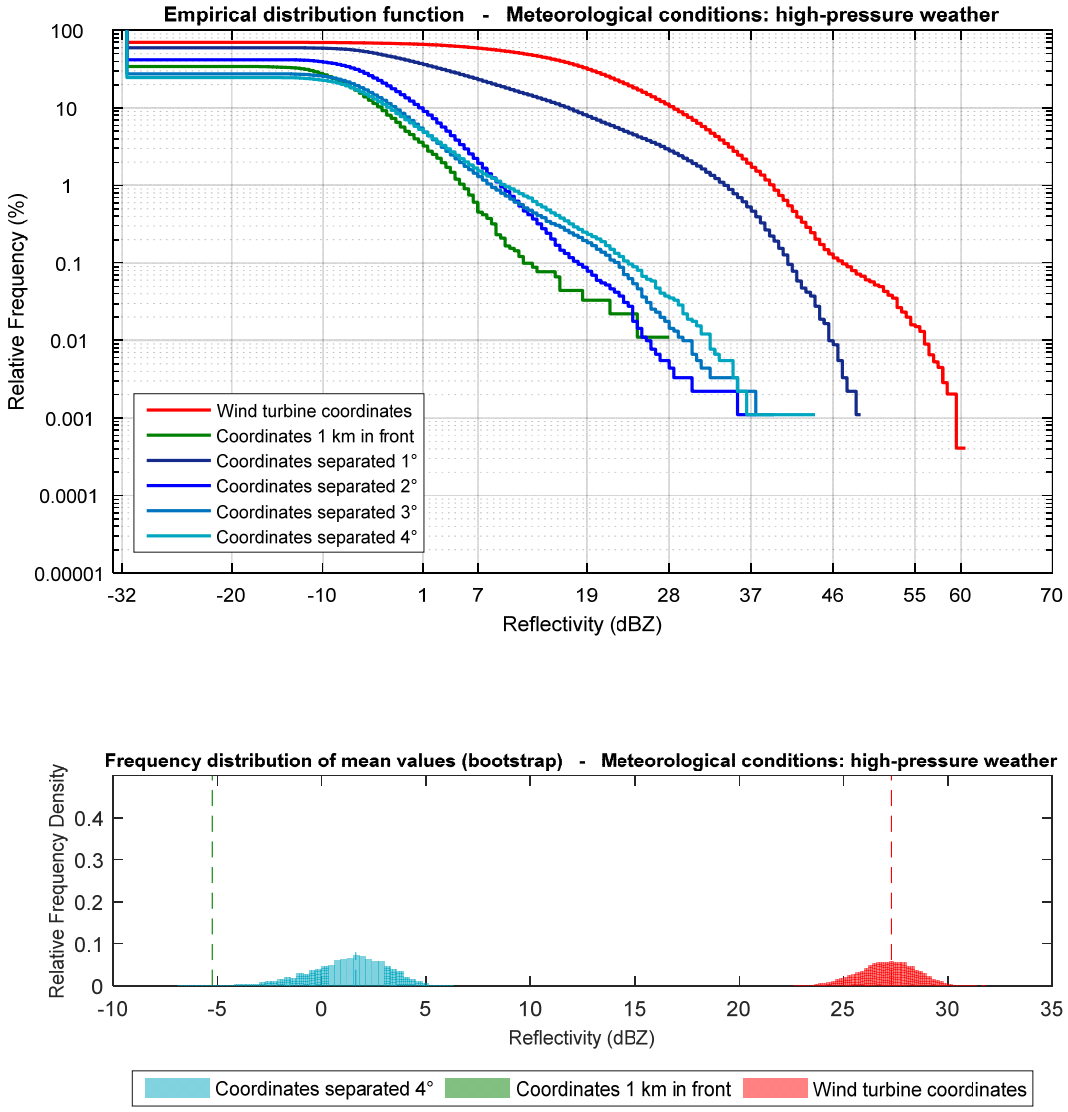


**Figure 38: Empirical CDF for measurements at defined coordinates and meteorological conditions; and bootstrap analysis of the mean values (below).**

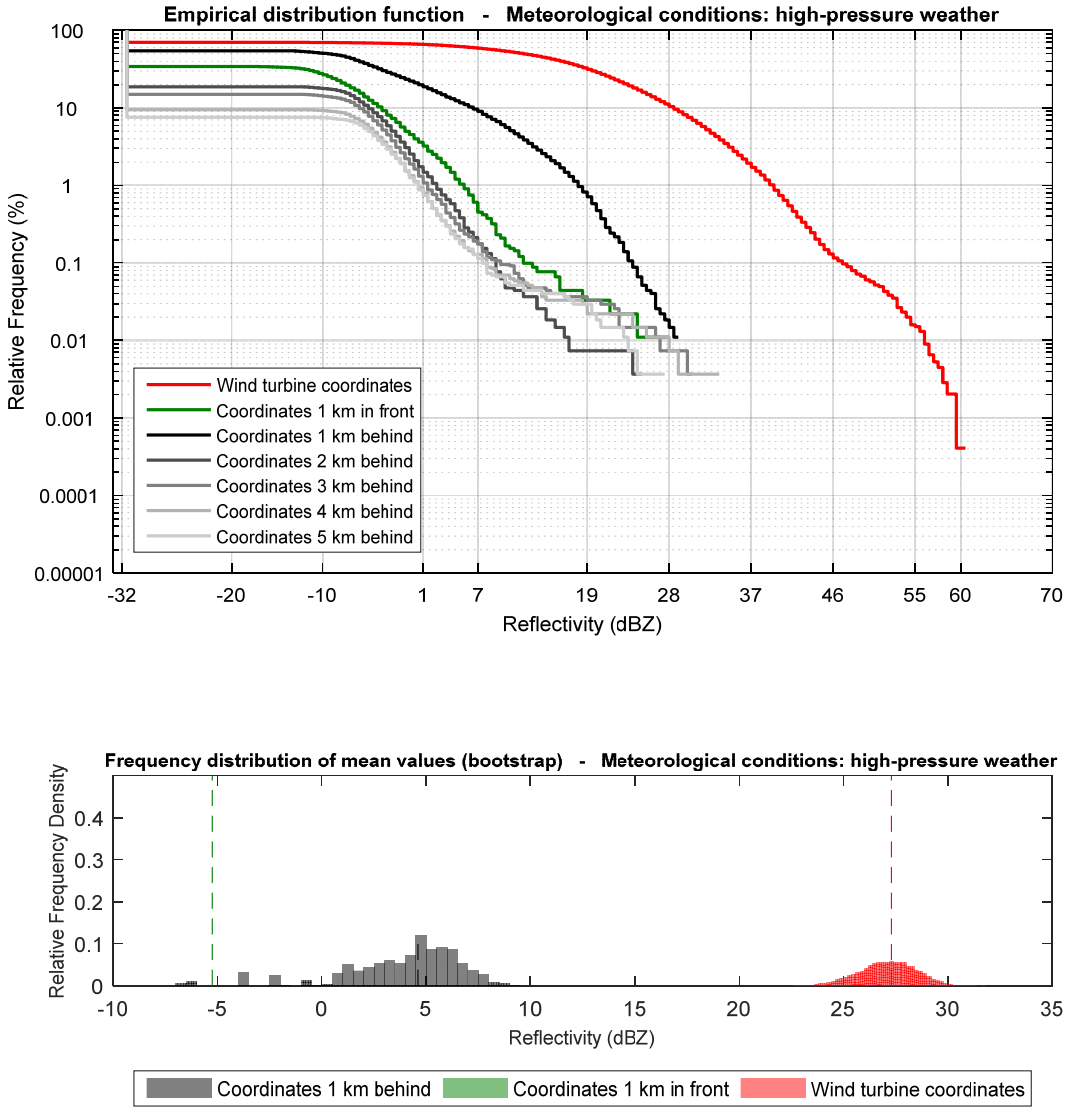


**Figure 39: Empirical CDF for measurements at defined coordinates and meteorological conditions; and bootstrap analysis of the mean values (below).**